

**STUDY OF OUT OF PLANE STRUCTURE OF IONIC POLYMER-METAL
COMPOSITES BASED SENSOR USING FINITE ELEMENT MODELLING**

MUHAMMAD TAUFIQ BIN HOOD

**A project report submitted in partial fulfilment of the requirements for the
award of Master of Engineering (Electronic Systems)**

**Lee Kong Chian Faculty of Engineering and Science
Universiti Tunku Abdul Rahman**

April 2019

DECLARATION

I hereby declare that this project report is based on my original work except for citations and quotations which have been duly acknowledged. I also declare that it has not been previously and concurrently submitted for any other degree or award at UTAR or other institutions.

Signature : _____

Name : MUHAMMAD TAUFIQ BIN HOOD

ID No. : 18UEM00855

Date : _____

APPROVAL FOR SUBMISSION

I certify that this project report entitled “**STUDY OF OUT OF PLANE STRUCTURE OF IONIC POLYMER-METAL COMPOSITES BASED SENSOR USING FINITE ELEMENT MODELLING**” was prepared by **MUHAMMAD TAUFIQ BIN HOOD** has met the required standard for submission in partial fulfilment of the requirements for the award of Master of Engineering (Electronic Systems) at Universiti Tunku Abdul Rahman.

Approved by,

Signature : _____

Supervisor : Dr. CHEE PEI SONG

Date : _____

The copyright of this report belongs to the author under the terms of the copyright Act 1987 as qualified by Intellectual Property Policy of Universiti Tunku Abdul Rahman. Due acknowledgement shall always be made of the use of any material contained in, or derived from, this report.

© 2019, Muhammad Taufiq Bin Hood. All right reserved.

ACKNOWLEDGEMENTS

I would like to thank everyone who had contributed to the successful completion of this project. I would like to express my gratitude to my research supervisor, Dr. Chee Pei Song for his invaluable advice, guidance and his enormous patience throughout the development of the research.

In addition, I would also like to express my gratitude to my loving parents and friends who had helped and given me encouragement to complete this project.

ABSTRACT

In this study, the simulation of cantilever beam design sensor using Ionic Polymer-Metal Composite (IPMC) is proposed. The simulation involved out-of-plane deformation force on IPMC cantilever sensor to define the characteristic of the sensor. IPMC is the material that creates a motion to electrical signals (sensor), where at the electrical signal generated from the mechanical movement of IPMC that cause form the migration of hydrated cations within the polymer structure. In this study, the sensor characteristic of cantilever IPMC design base on electromechanical movement and simulation by using COMSOL Multiphysics version 5.3 software to determine the electrical signal during force applied in eigenfrequency to the IPMC surface area to the variable IPMC height at 0.29 mm, 0.578 mm and 0.868 mm. The voltage signal was determined in the range of $-17\mu\text{V}$ to $2\mu\text{V}$ at the all IPMC height evaluated with the deformation of IPMC.

TABLE OF CONTENTS

DECLARATION	ii
APPROVAL FOR SUBMISSION	iii
ACKNOWLEDGEMENTS	v
ABSTRACT	vi
TABLE OF CONTENTS	vii
LIST OF TABLES	ix
LIST OF FIGURES	x
LIST OF SYMBOLS / ABBREVIATIONS	xiv

CHAPTER

1 INTRODUCTION	1
1.1 General Introduction	1
1.2 Importance of the Study	3
1.3 Problem Statement	3
1.4 Study Objectives	3
1.5 Scope and Limitation of the Study	3
1.6 Contribution of the Study	4
1.7 Outline of the Report	4
2 LITERATURE REVIEW	5
2.1 Introduction	5
2.2 Application of IPMC	5
2.3 Sensing Mechanism	15
2.4 IPMC physics-based transduction models	16
2.4.1 Governing equation: charge density and electric potential	16
2.4.2 Comparison between actuator and sensor.	17
2.5 Eigenfrequency analysis	18

2.6	Current Problem in IPMC	19
2.6.1	Decreasing solvent in IPMC.	19
2.6.2	Surface Resistance	19
2.7	Summary	20
3	METHODOLOGY AND WORK PLAN	21
3.1	Introduction	21
3.2	Software used	21
3.3	Simulation and Finite Element Method	21
3.4	COMSOL Simulation Steps	22
3.4.1	Choose Dimension	23
3.4.2	Add Physics	23
3.4.3	Geometry Modelling	24
3.4.4	Choose Study	25
3.4.5	Define Load/Terminals	25
3.4.6	Meshing	26
3.4.7	Define Study Steps and Compute	26
3.5	Summary	27
4	RESULTS AND DISCUSSIONS	28
4.1	Introduction	28
4.2	Simulation Result	28
4.2.1	0.29 mm IPMC height result	29
4.2.2	0.57 mm IPMC height result	37
4.2.3	0.86 mm IPMC height result	44
4.3	Summary	51
5	CONCLUSIONS AND RECOMMENDATIONS	52
5.1	Conclusions	52
5.2	Recommendations for future work	52
	REFERENCES	53

LIST OF TABLES

Table 2.1: Comparison table between actuator and sensor. (Stalbaum, Shen and Kim, 2016)	17
Table 3.1: Global Parameter (Pugal <i>et al.</i> , 2016).	23
Table 4.1: Eigenfrequency result	51

LIST OF FIGURES

Figure 1.1: IPMC mechanism in actuator and sensing (Shahinpoor, 2015).	2
Figure 1.2: Chemical molecular structure of (a) Flemion (b) Nafions, (c) perfluorinated compound.	2
Figure 2.1: Schematic of experiment. (Strazzeri <i>et al.</i> , 2009; Brunetto <i>et al.</i> , 2011)	5
Figure 2.2: 3D illustration design of omnidirectional IPMC sensor.(Lei, Sharif and Tan, 2016)	6
Figure 2.3: Line array design setup. (Abdulsadda and Tan, 2012)	7
Figure 2.4: Fish prototype with two type of IPMC design (A) Kepton webbing, (B) Sectored pectoral fin (Hubbard <i>et al.</i> , 2014).	7
Figure 2.5: Concept design of underwater micro robot (Abdelnour <i>et al.</i> , 2012).	8
Figure 2.6: Prototype illustration tactile of IPMC. (Bonomo <i>et al.</i> , 2008)	8
Figure 2.7: Tactile device experiment. (Brunetto <i>et al.</i> , 2010)	9
Figure 2.8: Illustration design of seismic sensor. (Andò <i>et al.</i> , 2013)	9
Figure 2.9: Valveless pump drug delivery. (Wang <i>et al.</i> , 2017)	10
Figure 2.10: IPMC diaphragm. (Nam and Ahn, 2012)	10
Figure 2.11: Concept design of microfluidic device. (McDaid <i>et al.</i> , 2012)	11
Figure 2.12: Terrestrial robot (Nguyen <i>et al.</i> , 2015).	11
Figure 2.13: (A) Compression mode, (B) Shear mode. (Gudarzi, Smolinski and Wang, 2017)	12
Figure 2.14: IPMC Palpatory pulse-rate extractor. (Chattaraj <i>et al.</i> , 2018)	12
Figure 2.15: Wormlike IPMC design. (Arena <i>et al.</i> , 2006)	13
Figure 2.16: Multi segment robot. (Wang <i>et al.</i> , 2015)	13

Figure 2.17: Movement of robot. (Wang <i>et al.</i> , 2015)	14
Figure 2.18: Concept design of IPMC fork clasper. (Feng and Huang, 2016)	14
Figure 2.19: Illustration design of IPMC arch shape actuator. (Feng and Yen, 2016)	15
Figure 2.20: Cantilever beam three eigenmode (COMSOL, 2018)	18
Figure 2.21: (a) High surface resistance without conductive metal on electrode, (b) Reduced surface resistance with conductive metal on electrode. (Bhandari, Lee and Ahn, 2012).	19
Figure 3.1: Comsol Multiphysics simulation flow chart.	22
Figure 3.2: 2D analysis dimension.	23
Figure 3.3: Manual material setting.	24
Figure 3.4: IPMC design.	24
Figure 3.5: Load boundary define on IPMC.	25
Figure 3.6: Terminals boundary define on IPMC.	25
Figure 3.7: 2D IPMC mesh.	26
Figure 3.8: Eigenfrequency study setting.	27
Figure 4.1: IPMC sensor Eigenfrequency at step mode 1 with result 4.86 Hz, (A) displacement field, m, (B) Electric potential, V.	29
Figure 4.2: IPMC sensor Eigenfrequency at step mode 2 with result 5.18 Hz, (A) displacement field, m, (B) Electric potential, V.	30
Figure 4.3: IPMC sensor Eigenfrequency at step mode 3 with result 30.52 Hz, (A) displacement field, m, (B) Electric potential, V.	31
Figure 4.4: IPMC sensor Eigenfrequency at step mode 4 with result at 32.74 Hz, (A) displacement field, m, (B) Electric potential, V.	32
Figure 4.5: IPMC sensor Eigenfrequency at step mode 5 with result at 85.72 Hz, (A) displacement field, m, (B) Electric potential, V.	33

Figure 4.6: IPMC sensor Eigenfrequency at step mode 6 with result at 93.82 Hz, (A) displacement field, m, (B) Electric potential, V.	34
Figure 4.7: Point load at point 10 mark location.	35
Figure 4.8: Point load at point 10 mark location graph.	35
Figure 4.9: Point load at point 11 mark location.	36
Figure 4.10: Point load at point 11 mark location graph.	36
Figure 4.11: IPMC sensor Eigenfrequency at step mode 1 with result at 9.34Hz, (A) displacement field, m, (B) Electric potential, V.	37
Figure 4.12: IPMC sensor Eigenfrequency at step mode 2 with result at 9.71Hz, (A) displacement field, m, (B) Electric potential, V.	38
Figure 4.13: IPMC sensor Eigenfrequency at step mode 3 with result at 58.55 Hz, (A) displacement field, m, (B) Electric potential, V.	39
Figure 4.14: IPMC sensor Eigenfrequency at step mode 4 with result at 61.07Hz, (A) displacement field, m, (B) Electric potential, V.	40
Figure 4.15: IPMC sensor Eigenfrequency at step mode 5 with result at 164.12 Hz, (A) displacement field, m, (B) Electric potential, V.	41
Figure 4.16: IPMC sensor Eigenfrequency at step mode 6 with result at 172.49Hz, (A) displacement field, m, (B) Electric potential, V.	42
Figure 4.17: Point load at point 10 mark location graph.	43
Figure 4.18: Point load at point 11 mark location graph.	43
Figure 4.19: IPMC sensor Eigenfrequency at step mode 1 with result at 13.90 Hz, (A) displacement field, m, (B) Electric potential, V.	44
Figure 4.20: IPMC sensor Eigenfrequency at step mode 2 with result at 14.39 Hz, (A) displacement field, m, (B) Electric potential, V.	45

- Figure 4.21: IPMC sensor Eigenfrequency at step mode 3 with result at 87.04 Hz, (A) displacement field, m, (B) Electric potential, V. 46
- Figure 4.22: IPMC sensor Eigenfrequency at step mode 4 with result at 90.27 Hz, (A) displacement field, m, (B) Electric potential, V. 47
- Figure 4.23: IPMC sensor Eigenfrequency at step mode 5 with result at 243.25 Hz, (A) displacement field, m, (B) Electric potential, V. 48
- Figure 4.24: IPMC sensor Eigenfrequency at step mode 6 with result at 253.16Hz, (A) displacement field, m, (B) Electric potential, V. 49
- Figure 4.25: Point load at point 10 mark location graph. 50
- Figure 4.26: Point load at point 11 mark location graph. 50

LIST OF SYMBOLS / ABBREVIATIONS

C	cation concentration, mol/m ³
μ	cation mobility, m ² /V.s
D	diffusion coefficient, m ² /s
F	Faraday's constant, C/mol
z	charge number
V_c	molar volume which quantifies the cation hydrophilicity
P	solvent pressure, Pa
ϕ	electric potential in the polymer, V

CHAPTER 1

INTRODUCTION

1.1 General Introduction

The flexibility of mechanical movement and low activation voltage are the inherent properties of ionic polymer metal composite (IPMC) which is in electroactive polymers (EAPs) family (Bar-cohen, 2004; Shahinpoor, 2015). IPMC was first introduced in 1997–1998 by Mohsen Shahinpoor, Yoseph Bar Cohen. The capability founded on research work supported by NASA–Jet Propulsion Laboratory (JPL)(Shahinpoor, 2015).

Ionic polymer metal composites (IPMC) consists of an ion migration polymer film (usually Nafion or Flemion) and two conducting materials as electrodes. Both electrodes are plated on both side of the ionic polymer film. Hydrated cations within IPMC under voltage potential or force and corresponding with electrostatic interaction which can act as an actuator or as a sensor (Bhandari, Lee and Ahn, 2012; Shahinpoor, 2015; Annabestani, Maymandi-Nejad and Naghavi, 2016). Actuator characteristic in IPMC happen due to voltage difference is applied across both plated electrodes, the IPMC will bend toward the positive side of the voltage applied and meanwhile IPMC as sensor creates a voltage difference when under mechanical or physical stress. The mechanism of sensing/energy harvesting in IPMCs due to migration of cations towards deformation-induced mechanical migration of cations towards boundary surfaces and generating a small voltage for most of small sample due to Poisson–Nernst–Planck phenomena (Porfiri, 2008; Shahinpoor, 2015).

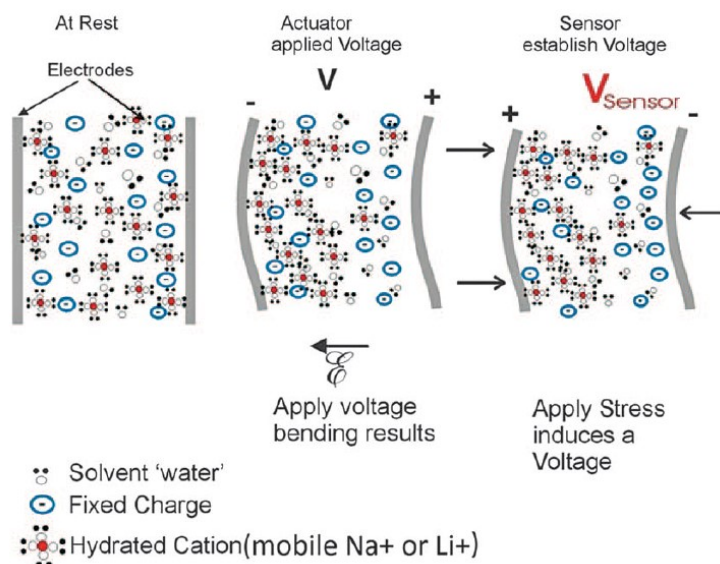


Figure 1.1: IPMC mechanism in actuator and sensing (Shahinpoor, 2015).

Common IPMC consist of a polyelectrolyte membrane (Nafion or Flemion). The ionic polymer widely used in IPMC technologies is Nafion and the electrodes are normally made from conductive material such as platinum, gold, silver, carbon composite. (Shahinpoor, 2016). The chemical molecular formulas of the Nafion, Flemion and perfluorinated compound shown in Figure 1.2.

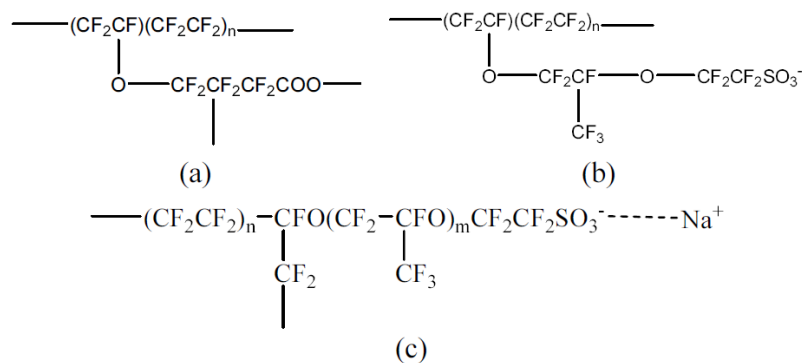


Figure 1.2: Chemical molecular structure of (a) Flemion (b) Nafions, (c) perfluorinated compound.

IPMCs as electroactive polymer (EAP) able work well in a liquid environment as well as in air and able to response at -100°C temperature. In other word IPMC able to operate as sensor and actuator under harsh condition (Shahinpoor *et al.*, 2009; Bhandari, Lee and Ahn, 2012).

1.2 Importance of the Study

IPMC in micro the electromechanical system (MEMS) as a sensor is important to detect the out of plane displacement of pressure/force. A MEMS sensor in medical will help to sense and differentiate the tissue hardness with the help of IPMC sensor mechanism. Sensor able to evaluate in real time physical characteristic of tissue in the human body which is to compare the stiffness of good tissue and tumor; example, some cancerous tissue such as breast, prostate, pulmonary and brain tumor area is harder than normal tissue. (Bonomo *et al.*, 2008; Thomas and Faouzi, 2016)

1.3 Problem Statement

Ionic Polymer Metal Composites (IPMC) display the bidirectional electromechanical movement that produced voltage output signal from out of plane movement position. However the voltage will produce different voltage value and this research will focus on the simulation of IPMC sensor using COMSOL is to determine the voltage signal at the out of plane motion.

1.4 Study Objectives

The study is to analyze the characteristic of IPMC sensor, which is to simulate the sensor output voltage when IPMC deflect out of plane motion using Comsol Multiphysics version 5.3 with built in finite element analysis.

The simulation to analysis the movement on each eigenfrequency of IPMC sensor and the electric potential along the sensor based on height (thickness) of IPMC.

1.5 Scope and Limitation of the Study

This study on IPMC is only limited to IPMC function as sensor. This report only study about characterizes of IPMC sensor. It is to understand how the IPMC sensor work, the response toward different motion and study on how to integrate IPMC into sensor application.

1.6 Contribution of the Study

The purpose of this research is to understand the properties of the IPMC to act as a sensor. The smart material as IPMC can be a sensor due to the movement stimulation (Bhandari, Lee and Ahn, 2012). The stability of the IPMC control is still difficult due to some of the chemical properties that can varies in IPMC. Hence, this research will help to clarify the properties of the IPMC in a simulation using COMSOL Multiphysics.

1.7 Outline of the Report

This report is consists of the literature review on the materials studied by other researches. IPMC model was simulated using finite elements analysis method. Studies on IPMC sensor capability and current voltage response were conducted to understand the characteristics of IPMC sensor.

CHAPTER 2

LITERATURE REVIEW

2.1 Introduction

This chapter previous research paper that relevant to this study. Some researchers studied about the IPMC sensor characteristic to detect the voltage or current signal on the specific position of pressure on IPMC. The previous research also investigated the IPMC sensor application that makes them improve the current application in very different fields such as in robotics, medical, and seismic sensor.

2.2 Application of IPMC

The IPMC can be actuator or sensor, the application that used IPMC such as in robotic both on land and in water (Shahinpoor *et al.*, 1998), medical tools application and remote sensing (geoscience).

A Study from Brunetto *et al.*, 2011, to characterize the IPMC based on the temperature and humidity influences (Strazzeri *et al.*, 2009). The research done on physical IPMC with different of relative humidity and temperature condition (Brunetto *et al.*, 2011). Result showed humidity plays a big role on the IPMC sensor characteristic than temperature (Brunetto *et al.*, 2011). This finding showed that external humidity environment such as biomedical and underwater is suitable for IPMC sensor. The experiment setup as shown as Figure 2.1.

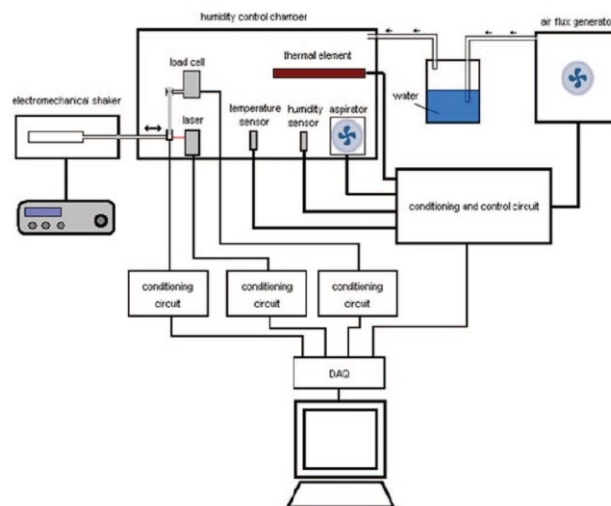


Figure 2.1: Schematic of experiment. (Strazzeri *et al.*, 2009; Brunetto *et al.*, 2011)

Research on omnidirectional IPMC sensor done by Lei, Sharif and Tan, 2016 by fabricating tubular IPMC with inner common electrode inside and four at outside the tubular IPMC sensor. This research is to determine the sensing capability at any direction and operational effectiveness of the omnidirectional sensor in an open air environment. The four outside tubular IPMC electrodes are to detect all external force from any direction which the movement produced electrical signal on each electrode, which the electrical signal will give result to determine the actual force direction on the IPMC (Lei, Sharif and Tan, 2016). The omnidirectional sensor design as shown as Figure 2.2.

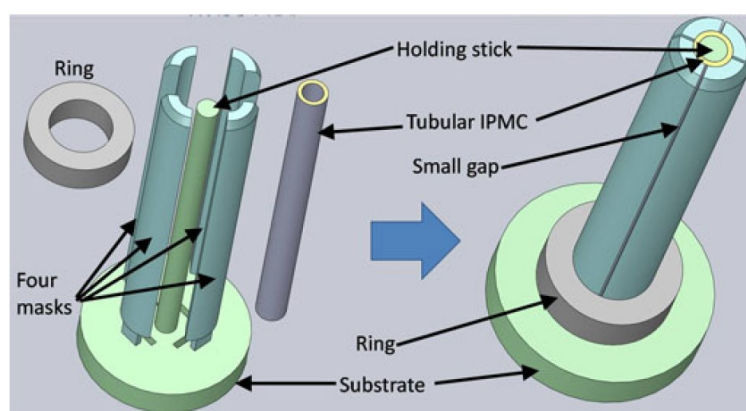


Figure 2.2: 3D illustration design of omnidirectional IPMC sensor.(Lei, Sharif and Tan, 2016)

IPMC line arrays sensor research by Abdulsadda and Tan, 2012, is to detect in water environment such as wave and water movement. This array sensor is acting as neuromasts on aquatic to probe their environment (Coombs and Braun, 2003; Abdulsadda and Tan, 2012). The vibrator that generate wave located at various location in a small tank and sensor will detect the wave generated. This research is suitable for under water robotic application such as self-propelled submarines. The design setup as shown as Figure 2.3.

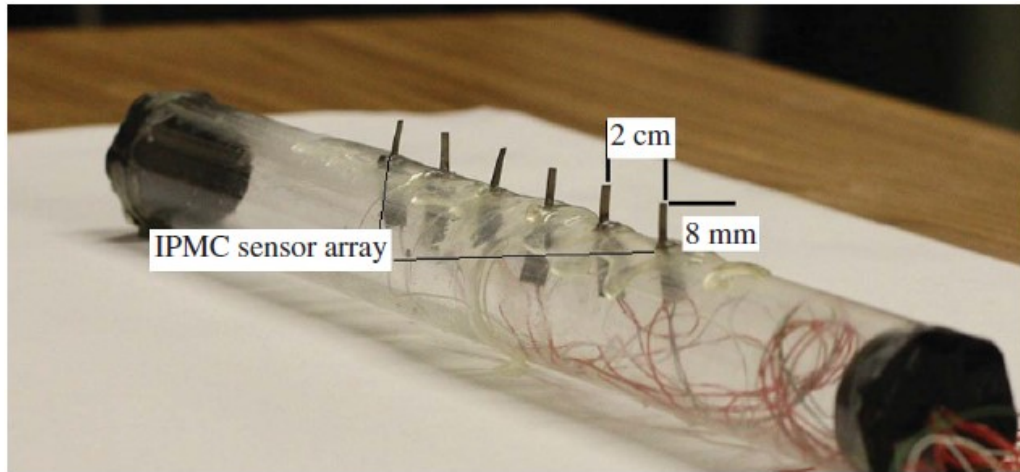


Figure 2.3: Line array design setup. (Abdulsadda and Tan, 2012)

Robotic application is wide IPMC used such as in water, fish fin using IPMC by Hubbard *et al.*, 2014. The study is about the design of fish fin by using IPMC to make maneuverable fish robot in water. The movement IPMC consists twisting, flapping and bending to act as fish maneuverable biological. The torque and tip force exceed 16.5mN at 3V and twisting angle exceeds 8° . The author reported it can move at 22 mm/s in the experimental test (Hubbard *et al.*, 2014). The prototypes as shown in Figure 2.4.

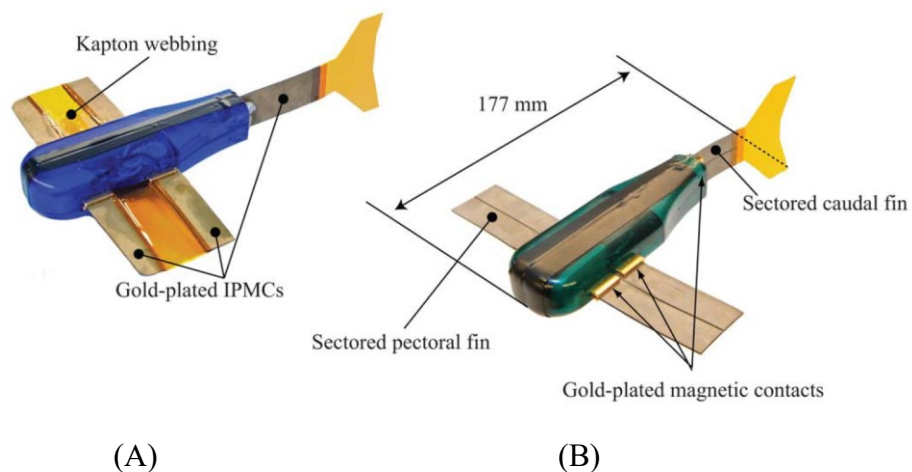


Figure 2.4: Fish prototype with two type of IPMC design (A) Kepton webbing, (B) Sectored pectoral fin (Hubbard *et al.*, 2014).

Wireless power supply using magnetic coupling coil to power the IPMC actuator. The experiment done by Abdelnour *et al.*, 2012, by compared the movement of IMPC in water with direct supply power. The result of the experiment was comparable between wireless and direct supply to IPMC by capture the movement characteristic of IPMC. The concept of underwater micro robot as shown at Figure 2.5.

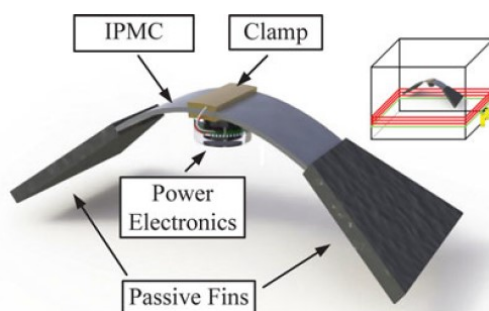


Figure 2.5: Concept design of underwater micro robot (Abdelnour *et al.*, 2012).

There are multiple multifunction design of tactile device designed to fulfill medical needs (Hemsel *et al.*, 2007), In Bonomo *et al.*, 2008 research, IPMC tactile sensor for biomedical application used two IPMC strips, one of it as a sensor and another as an actuator. These two IPMC works together to sense material in contact (sensing) with the IPMC sensor mechanism part. The IPMC actuator function is to generate a movement to IPMC sensor to control the actuator grip strength in medical application to sensing tissue stiffness (Bonomo *et al.*, 2008; Thomas and Faouzi, 2016). The study mention needs to improve on a sensing tip of sensor for exploration purpose of the area surrounding. Medical equipment needs to be sensitive to important organ in human in operation procedure. This will avoid sensor damaging the organ. The design of experiment shown as Figure 2.6.

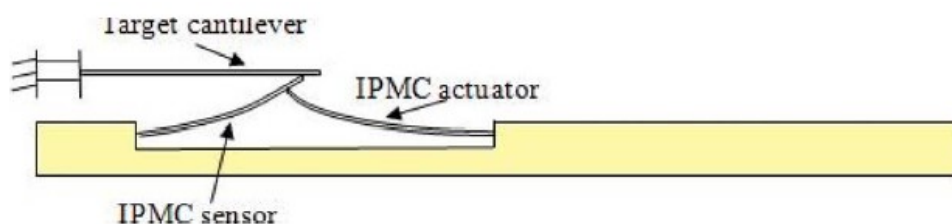


Figure 2.6: Prototype illustration tactile of IPMC. (Bonomo *et al.*, 2008)

The tactile device experiment is the actuator part give a resonant condition on the sensor. This the resonant condition created same frequency from actuator to sensor (Macquarie University, 2009). The experiment done to recognize contact material in two condition water and open air, where the result is by comparing the phase and magnitude (Brunetto *et al.*, 2010). Tactile experiment device as shown in Figure 2.7.

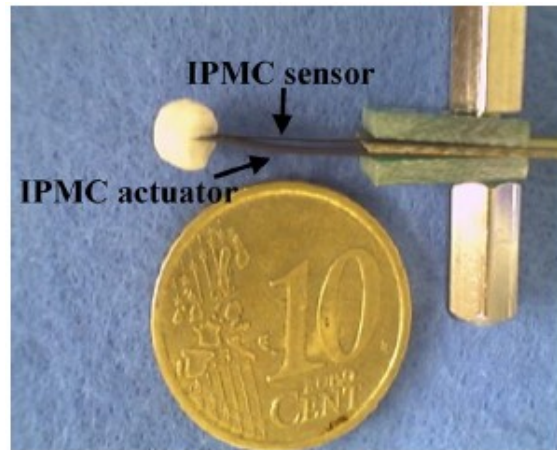


Figure 2.7: Tactile device experiment. (Brunetto *et al.*, 2010)

Andò *et al.*, 2013, is about seismic sensor with a combination of IPMC sensor and ferrofluids. The IPMC sensor beam immersed in vial filled with ferrofluids, operate as the seismic mass. Inertial stimulus applied to the transducer and produced an electrical signal (Andò *et al.*, 2013). The study is to determine the sensor behavior and characteristic to ferrofluid density and open air condition. Seismic illustration design as shown as Figure 2.8.

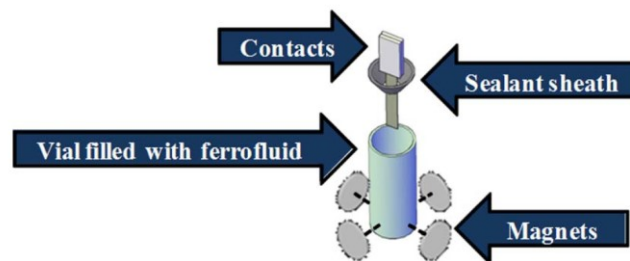


Figure 2.8: Illustration design of seismic sensor. (Andò *et al.*, 2013)

Wang *et al.*, 2017 studied about drug delivery valveless pump using IPMC as actuator to push diaphragm. The large IPMC deflection will force diaphragm drug to flow out from chambers. The study was done by operated the IPMC actuator at 2 hours repetitive movement to validate the suitability in drug delivery pump system. The result shows the IPMC at maximum deflection can delivered 780 $\mu\text{L}/\text{min}$ (Wang *et al.*, 2017). The prototype illustration design as shown at Figure 2.9.

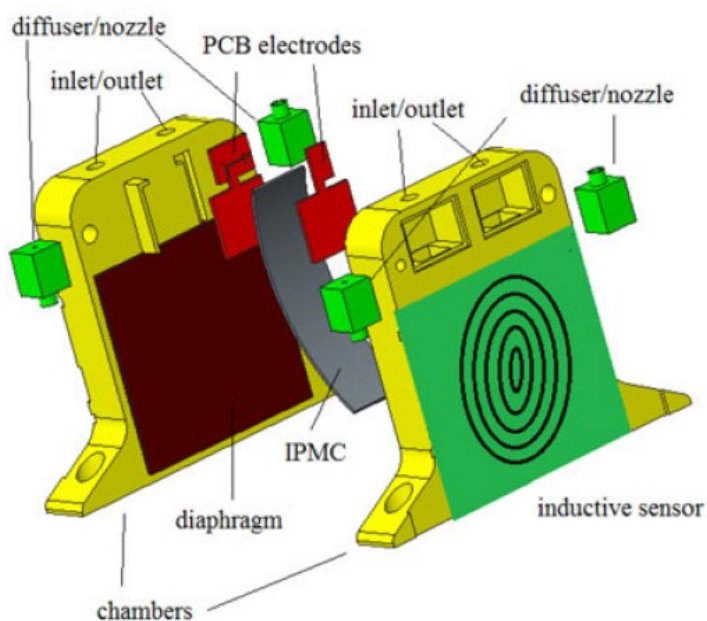


Figure 2.9: Valveless pump drug delivery. (Wang *et al.*, 2017)

Valveless method can improve by applying the IPMC in the diaphragm to deliver the drug (Ngoc *et al.*, 2012). The IPMC simulation in diaphragm divided into four to maximize the deflection for maximum drug delivery. Design of IPMC diaphragm as shown in Figure 2.10.

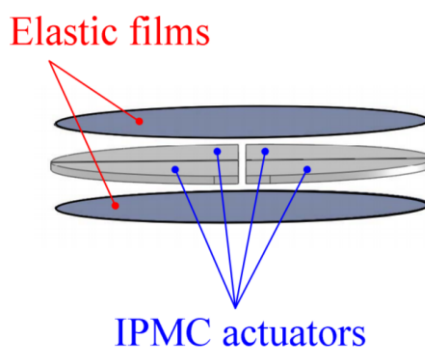


Figure 2.10: IPMC diaphragm. (Nam and Ahn, 2012)

A study by McDaid *et al.*, 2012, microfluidic simulation using Iterative Feedback Tuning (IFT). Author said the system is to have a reliable performance without having an offline tuning. The finding showed it has better 92% than a conventional tuned controller. The Figure 2.11 is the concept of microfluidic device.

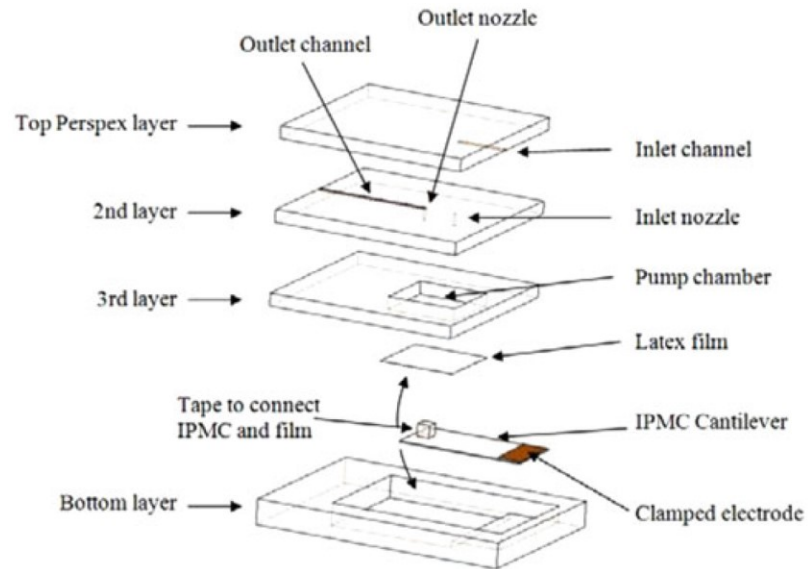


Figure 2.11: Concept design of microfluidic device. (McDaid *et al.*, 2012)

The robotic application on land by using two degree of freedom (2DoF) on terrestrial walking robot to improve the movement of the robot with Polydimethylsiloxane (PDMS) covered IPMC robot leg (Nguyen *et al.*, 2015). The PDMS coverage increase the friction force on the actuator with helps of 2DoF which increase the displacement of robot leg. The design illustration as shown at Figure 2.12.

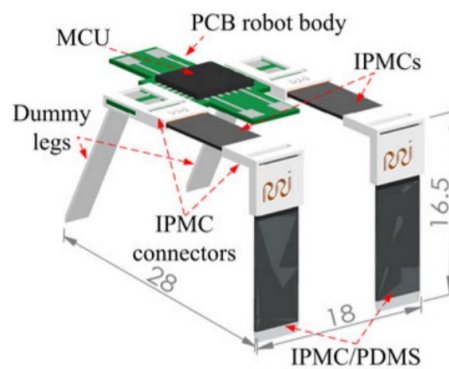


Figure 2.12: Terrestrial robot (Nguyen *et al.*, 2015).

A research on pressure sensor, comparison between compression mode and shear mode sensor done by Gudarzi, Smolinski and Wang, 2017. The experiment done in shock tube to utilize the result on both compression and shear mode. The result showed the shear mode sensor had high sensitivity than compression mode by 1.6 factor. Illustration design of sensor as shown in Figure 2.13.

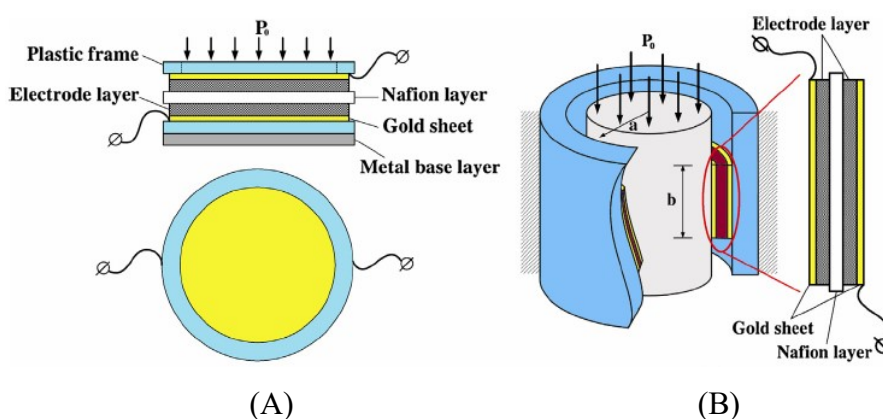


Figure 2.13: (A) Compression mode, (B) Shear mode. (Gudarzi, Smolinski and Wang, 2017)

Pulse rate extractor research based on IPMC done by Chattaraj *et al.*, 2018, to extract pulse at human wrist. The pulse from wrist detected by sensor and produced electrical signal which compared to the digital stethoscope. The error percentage result around 4-15%. The pulse rate extractor as shown in Figure 2.14.

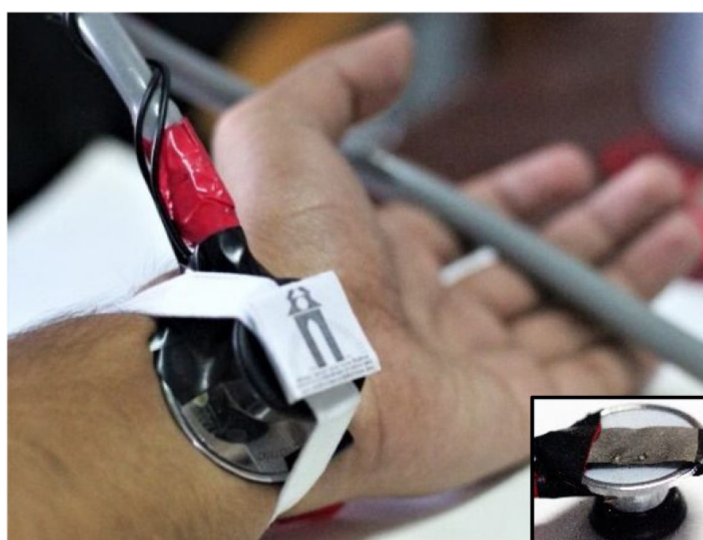


Figure 2.14: IPMC Palpatory pulse-rate extractor. (Chattaraj *et al.*, 2018)

Robotic technology, mostly imitating real life living creature on earth (Manuel and Voth, 2014). In research by Arena *et al.*, 2006, IPMC used to build a wormlike robot. The design used cellular neural networks (CNNs) to control each segment on the polymer membrane where each segment covered with metal electrode (Arena *et al.*, 2006). This method to create the undulation movement on wormlike robot (Ostrowski and Burdick, 1998). Design of the wormlike robot as shown in Figure 2.15.

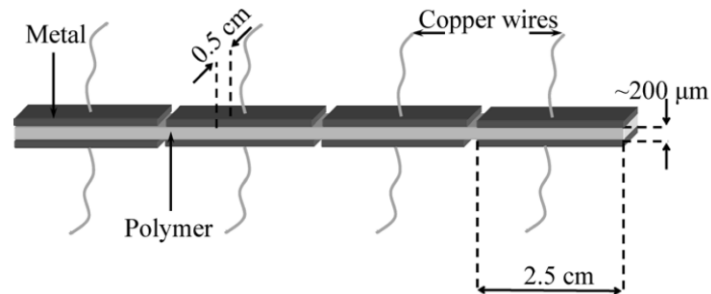


Figure 2.15: Wormlike IPMC design. (Arena *et al.*, 2006)

Multi segment robot in Wang *et al.*, 2015 research is to encounter the path obstacle by the soft membrane such as IPMC (Trivedi *et al.*, 2008) shown in Figure 2.16. Gaussian model used in the robot design (Wang *et al.*, 2015) resulting it can pass the obstacle path as shown in Figure 2.17.

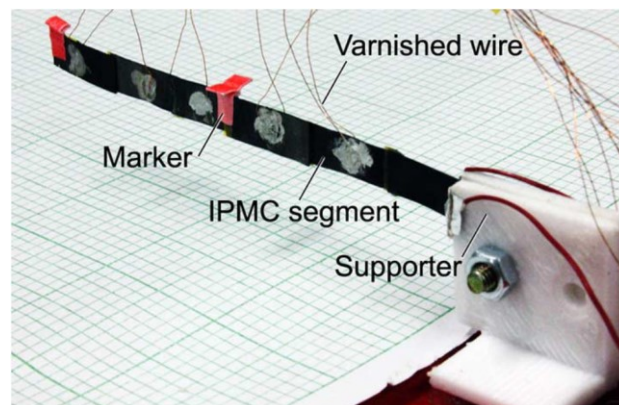


Figure 2.16: Multi segment robot. (Wang *et al.*, 2015)

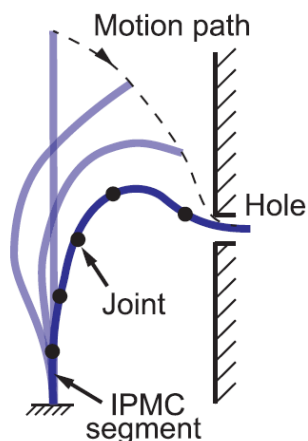


Figure 2.17: Movement of robot. (Wang *et al.*, 2015)

The fork shape gripper based on IPMC actuator with strain gage for sensing and ultrasonic imaging was studied by Feng and Huang, 2016. The gripper has the ability to do ultrasonic imaging, where generated ultrasonic waves can penetrate the sample by using liquid as transfer medium (HDI Solution INC, 2016). Sensing mechanism in gripper used soft strain gage to integrate with soft gripper for smooth movement (Feng and Huang, 2016). The result showed the signal imaging and sensing operate as author wanted. The concept of design shown in Figure 2.18.

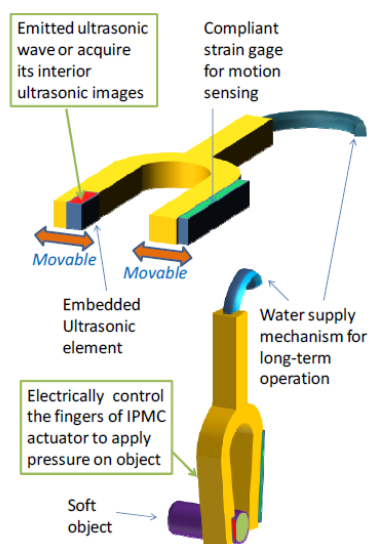


Figure 2.18: Concept design of IPMC fork clammer. (Feng and Huang, 2016)

The arch shape IPMC actuator was studied by Feng and Yen, 2016, to hold scissor gripper and operate it. The study done by fabricating the arch actuator with a hinge at the end of both tip. The experiment was done on the fabricated arch to determine the displacement gap of the both hinge, then continue with a displacement of the scissor gripper experiment. The result in the experiment shows the both sides had symmetry movement by plotting the signal graph. The illustration of arch actuator shown in Figure 2.19.

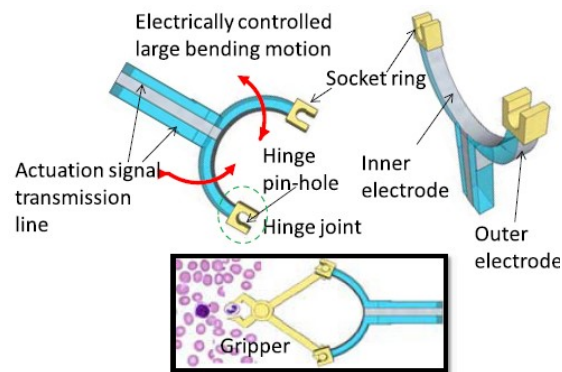


Figure 2.19: Illustration design of IPMC arch shape actuator. (Feng and Yen, 2016)

2.3 Sensing Mechanism

The sensing mechanism is the mechanical pressure applied on IPMC and induced the ion diffusion. This pressure mechanism produced an electric potential in the low time period at the both side IPMC of electrodes. (Shahinpoor, 2015; Chattaraj *et al.*, 2018).

From Nernst–Planck formula, cations transfer to one region of the membrane and producing an electrical signal (Shahinpoor, 2015), which at reverse side cause the ion diffusion from phenomena of ion concentration difference. This event makes ions to disperse evenly across the membrane to uphold a balance condition (Shahinpoor, 2015).

Charge dynamic integrating with mechanical force design by an equation that correlates the ion concentration from the osmosis pressure. In macro scale design, this correlation gives effect to the output of IPMC sensor on difference mechanical force mode (Shahinpoor, 2015; Chattaraj *et al.*, 2018). Micro scale models are required to take involve the effects of developed strain mode structure which are tension, bending and twisting on the permeable media, including effects on the contraction and expansion of the membrane and ion species diffusion micro-channels (Shahinpoor, 2015).

2.4 IPMC physics-based transduction models

IPMC sensor is mechanoelectrical event that inverse from actuator. It is important to understand clearly that the underlying cause of both of the phenomena of sensor and actuator, is resulting non-zero space charge and induced ionic current and in the region of the electrodes. Nernst–Planck equation used to calculate the ionic current (Pugal *et al.*, 2016):

$$\frac{\partial C}{\partial t} + \nabla \cdot \left(\underbrace{-D\nabla C}_{\substack{\text{diffusive} \\ \text{cation flux}}} - \underbrace{z\mu FC\nabla\phi}_{\substack{\text{migration} \\ \text{in elec. field}}} - \underbrace{\mu CV_C\nabla P}_{\substack{\text{convective} \\ \text{cation flux}}} \right) = 0 \quad (2.1)$$

Mobility can be explicitly expressed as (Pugal *et al.*, 2016):

$$\mu = \frac{D}{RT} \quad (2.2)$$

Where R is the gas constant and T is the absolute temperature.

The electric potential gradient term is significantly more common than the solvent pressure flux, that is:

$$zF\nabla\phi \gg V_C\nabla P \quad (2.3)$$

In actuation implementation model neglected on the pressure flux term is often happen. However, the pressure flux term in sensing situation case are significance and neither should be neglected (Stalbaum, Shen and Kim, 2016).

2.4.1 Governing equation: charge density and electric potential

Main governing equation of Nernst-Planck equation to describing the transduction process of the IPMC materials. The equation consists of three flux terms governed by different field gradients, namely electric potential gradient $\nabla\phi$, concentration gradient ∇C , and solvent pressure gradient ∇P (Pugal *et al.*, 2016).

Description by Poisson's equation below in term of electric potential:

$$-\nabla^2 \phi = \frac{\rho}{\varepsilon} \quad (2.3)$$

The charge density, ρ and absolute dielectric permittivity, ε defined as:

$$\rho = F(C - C_a) \quad (2.4)$$

Relation of anion concentration C_a to volumetric strain as:

$$C_a = C_0 \left[1 - \left(\frac{\partial u_1}{\partial x} + \frac{\partial u_2}{\partial y} + \frac{\partial u_3}{\partial z} \right) \right] \quad (2.5)$$

2.4.2 Comparison between actuator and sensor.

The comparison between actuator and sensor is where the actuator generates movement applied the voltage and the sensor generated electrical signal as load applied on the sensor. The comparison Table 2.1 shown below explains that the sensor need to consider the convective flux in the mechanoelectrical sensing mechanism.

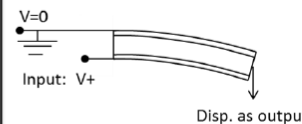
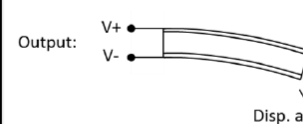
Transduction mechanism	Electromechanical (Actuation)	Mechanoelectrical (Sensing)
Illustration of input / outputs	 <p>Input: V+ Disp. as output</p>	 <p>Output: V+ V- Disp. as input</p>
Flow diagram of modeling approach	<p>input: electrode voltage</p> <p>↓</p> <p>Nernst-Planck and Poisson's Equations</p> <p>↓ ρ_c, F</p> <p>Solids model</p> <p>↓</p> <p>output: u, v, w, x, y, z</p>	<p>input: displacement</p> <p>↓</p> <p>Solids model</p> <p>↓ u, v, w, x, y, z, σ</p> <p>Nernst-Planck and Poisson's Equations</p> <p>↓</p> <p>output: C, C_a, ϕ, V</p>
Important differences	$C_a \approx C_0$ $zF\nabla\phi \gg \Delta V / \bar{V}$	$C_a = C_0 \left[1 - \left(\frac{\partial u_1}{\partial x} + \frac{\partial u_2}{\partial y} + \frac{\partial u_3}{\partial z} \right) \right]$ <i>Convective flux considered</i>

Table 2.1: Comparison table between actuator and sensor. (Stalbaum, Shen and Kim, 2016)

2.5 Eigenfrequency analysis

Eigenfrequencies where the analysis involved natural frequencies. There are certain frequencies at which a system is forced to vibrate. These frequencies produced in many ways, for example, in an electrical RLC circuit or a musical instrument (COMSOL, 2018).

The structure can deform when it vibrating at a certain eigenfrequency. The shape of mode only provided by an eigenfrequency analysis, not the amplitude of any physical vibration.

In continuous system there are infinite eigenfrequencies, but only few mode taken to do the analysis (AMRITA, 2011; COMSOL, 2018). The equation of orthogonality mode can be expressed as:

$$\int_V \rho u_i \cdot u_j dV = \delta_{ij} \quad (2.7)$$

Where u is displacement, ρ is density, Eigenfrequency for beam can expressed as:

$$\omega_m = k_{s,m} \frac{1}{L^2} \sqrt{\frac{EI}{\mu}} \quad (2.7)$$

L is beam length, EI is bending constant and μ is mass per unit length. Where $k_{s,m}$ for fix free cantilever beam as below:

$$k_{s,m} = \left(\left(m - \frac{1}{2} \right) \pi \right)^2 \quad (2.8)$$

The fix free cantilever beam with three mode in eigenfrequency as shown in Figure 2.20.

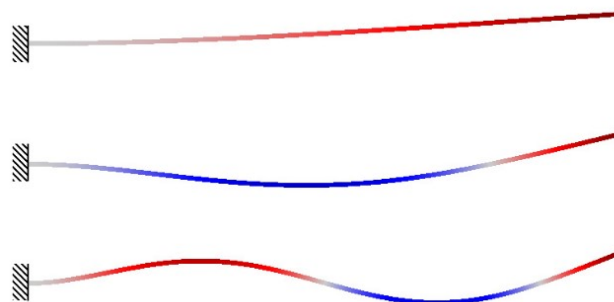


Figure 2.20: Cantilever beam three eigenmode (COMSOL, 2018)

2.6 Current Problem in IPMC

2.6.1 Decreasing solvent in IPMC.

The ions move with the solvent molecules and in Deionized water (DI) is used as solvent. Decreasing solvent are either happen due to evaporation or electrolysis. In conventional IPMC, H^+ is commonly used in hydrolysis, which H^+ tend to improve the IPMC force characteristic instead of Li^+ and Cu^+ (Bhandari, Lee and Ahn, 2012)

2.6.2 Surface Resistance

Surface resistance in IPMC play important role in deformation structure. The repetition of contraction and relaxation on IPMC surface during bending create cracks and worsen the surface conductivity on electrode surface (Bhandari, Lee and Ahn, 2012). When the high conductive metal coated on electrode, the cation and solvent molecules move evenly along the IPMC thickness as shown in Figure 2.21.

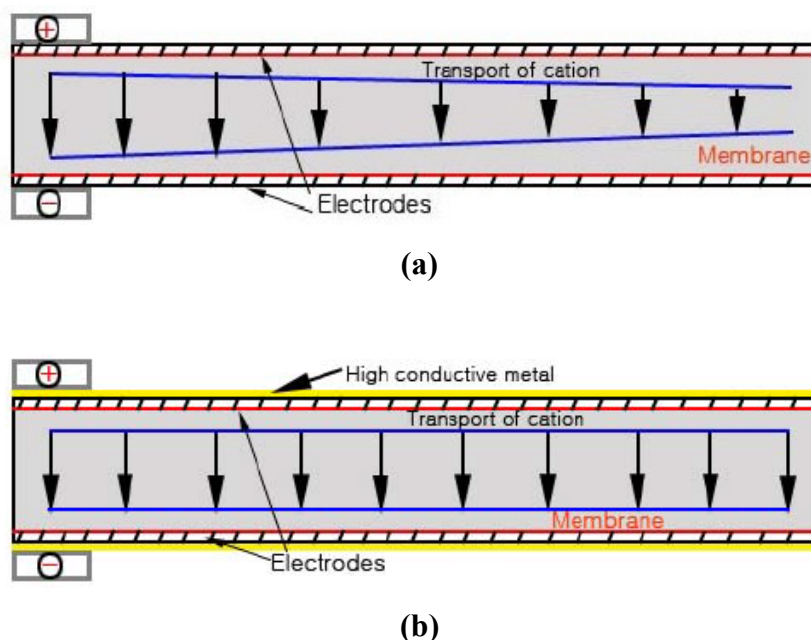


Figure 2.21: (a) High surface resistance without conductive metal on electrode, (b) Reduced surface resistance with conductive metal on electrode. (Bhandari, Lee and Ahn, 2012).

2.7 Summary

The IPMC is the multi-function material that can be an actuator and sensor. Focus need be more on sensor since the IPMC research mostly on the actuator. The good side of IPMC sensor is the sensitivity of membrane, low actuating voltage (Tsiakmakis *et al.*, 2009) with large deflection and biocompatibility (Bar-cohen, 2002; Wang *et al.*, 2017). The studies about sensor will improve the characteristic of IPMC in future applications.

CHAPTER 3

METHODOLOGY AND WORK PLAN

3.1 Introduction

Design that involved in this study is IPMC sensor cantilever with finite element method. The IPMC cantilever included the terminal clamping at the each side end of cantilever.

3.2 Software used

In this study, COMSOL Multiphysics version 5.3 is used for couple analysis because of the interactive and user friendly for modelling and meshing. This software also used for modelling and optimization with Solid Mechanics module, electrical module and mesh module involved.

3.3 Simulation and Finite Element Method

Finite element method was conducted using COMSOL Multiphysics to evaluate the performance of the sensor. The mathematics equation that build in inside the Comsol Multiphysics make the software friendly to user. The objective of this simulation is to study the sensor out of plane displacement and force interaction to produce voltage signal for cantilever IPMC. The second objective is to determine the resonance frequency that produce from the free movement IPMC beam after single load struck.

The simulation was chosen to be in 2D as the study is to translational force and displacement in XY plane which the model applies a force to cantilever that create movement and produce voltage signal.

The design of cantilever IPMC sensor will consist the IPMC membrane and clamping electrodes. Physics that involved are Solid Mechanical and Electromechanical, which compute with Eigenfrequency study.

3.4 COMSOL Simulation Steps

The design of 2D IPMC sensor by using Comsol Multiphysics version 5.3 is consist the physics applied to measure operation of design based on parameter definition. Study application applied to run the simulation and generate the result for analysis. Figure 3.1 is the flow chart of the cantilever IPMC sensor simulation design using Comsol Multiphysics version 5.3.

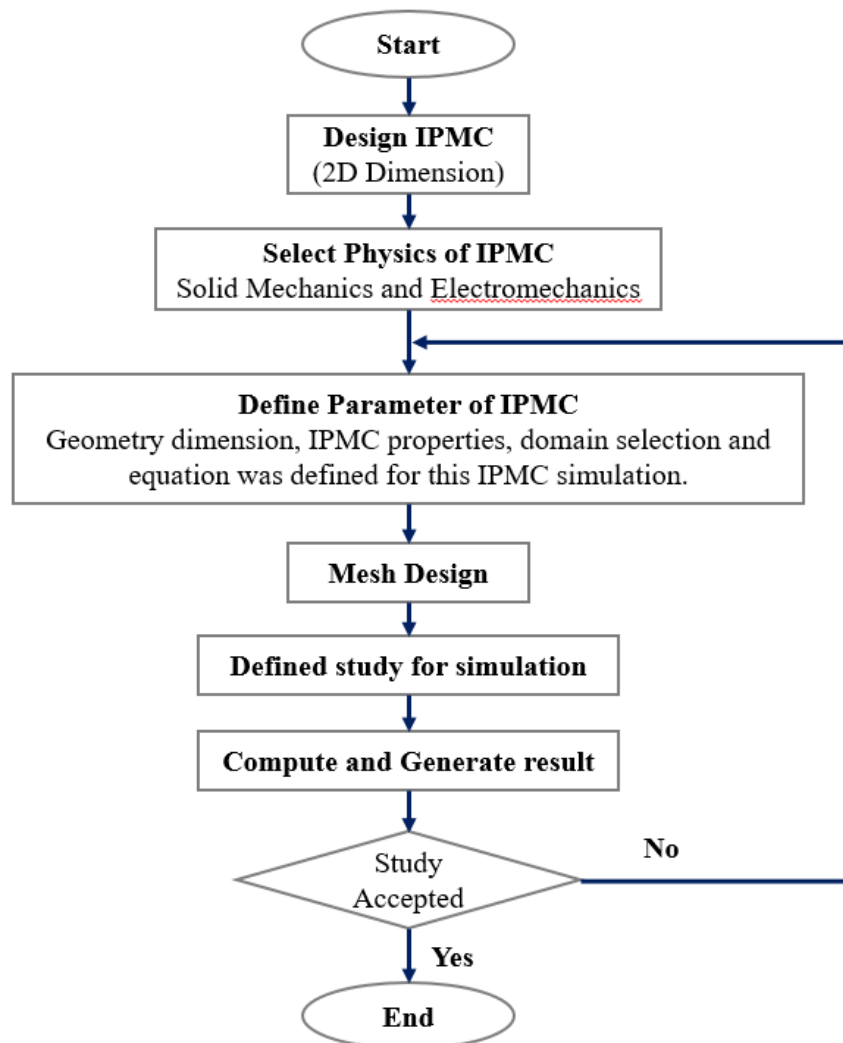


Figure 3.1: Comsol Multiphysics simulation flow chart.

3.4.1 Choose Dimension

First step for using COMSOL Multiphysics to define the dimension. This study used 2D analysis dimension as shown in figure 3.2. 2D analysis can minimized memory consumption and reduce computational duration by reducing the number of meshing element.

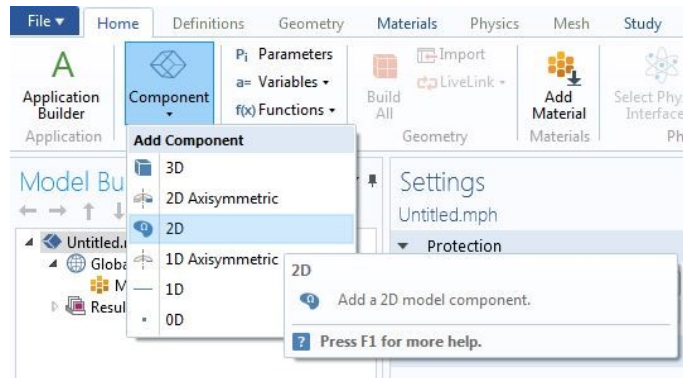


Figure 3.2: 2D analysis dimension.

3.4.2 Add Physics

The second step is adding the governing equation involve in the simulation process. The physics used in this study are Solid Mechanics and Electromechanics which all finite element method formula already build in the each physics. Solid Mechanics is to drive the load to the IPMC sensor and Electromechanics is to detect the voltage signal from the movement of IPMC after load applied. Material defined manually in the both Solid Mechanics and Electromechanics physics by using Table 3.1 parameters for IPMC in Global Parameter in COMSOL from (Pugal *et al.*, 2016). Figure 3.3 is the manual setting for material.

Name	Expression
Young_IPMC	41[MPa]
Poisson_IPMC	0.49
density_IPMC	2000[kg/m ³]

Table 3.1: Global Parameter (Pugal *et al.*, 2016).

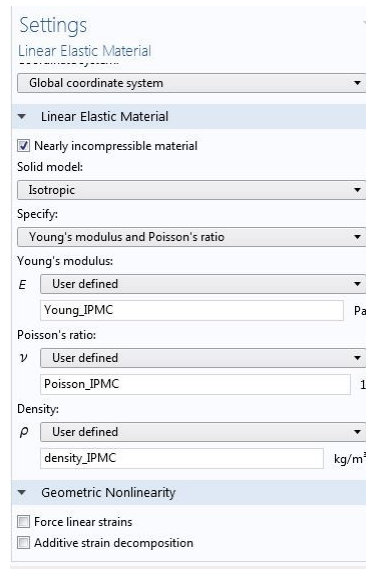


Figure 3.3: Manual material setting.

3.4.3 Geometry Modelling

The geometry model for this study using cantilever IPMC sensor as shown in Figure 3.2. The design has 1 IPMC membrane and 2 electrode for clamping, which combination both divided into two segment, one for terminal clamping (left) and free movement (right) as shown in figure 3.3. The length of IPMC is 51.07 mm and the height is compared with 4 of value 0.29 mm, 0.57 mm and 0.86 mm. The electrode size is 51.07 mm in length and 0.008 mm height clamping on top and bottom IPMC. The terminals clamping and free movement region was divided with boundary between regions.

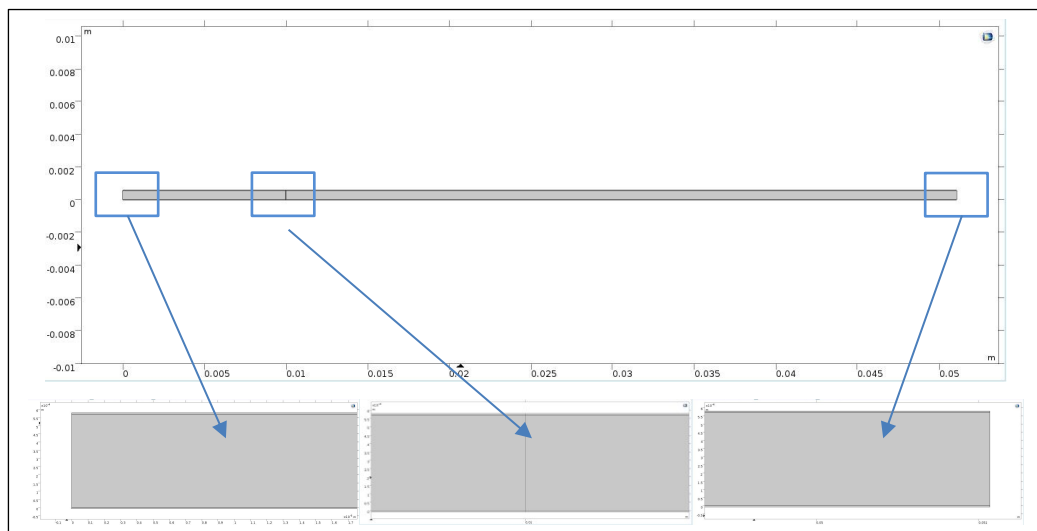


Figure 3.4: IPMC design.

3.4.4 Choose Study

The study type in this simulation is define as Eigenfrequency where eigenfrequency number been set to 6 mode step. The frequency, displacement and voltage signal will compute in this study.

3.4.5 Define Load/Terminals

In physics, load on IPMC defined in Solid Mechanics physics the load applied on boundary as shown in Figure 3.5. The load applied with 200Pa on boundary.



Figure 3.5: Load boundary define on IPMC.

Terminals been defined in Electromechanics physics at the clamping area with positive and negative terminals as shown in figure 3.6. Both terminals was set limit at 1V and -1V for each positive and negative terminals.

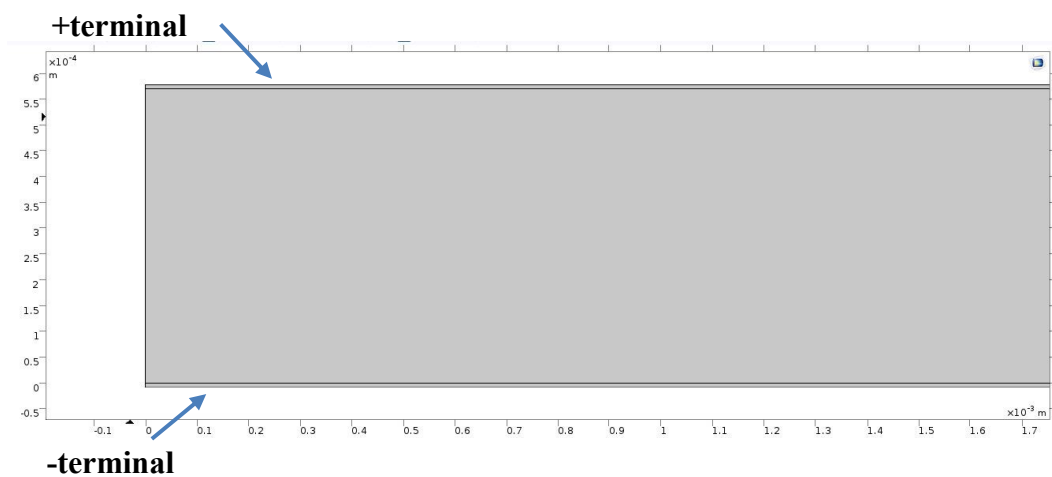


Figure 3.6: Terminals boundary define on IPMC.

3.4.6 Meshing

The meshing process can be carried out simultaneously for multiple analyses and automatically generated. In this study the mesh applied manually at the edge of terminals clamping area with edge type mesh and distribution. It follow by applied mapped mesh on remaining boundary as shown in Figure 3.7.

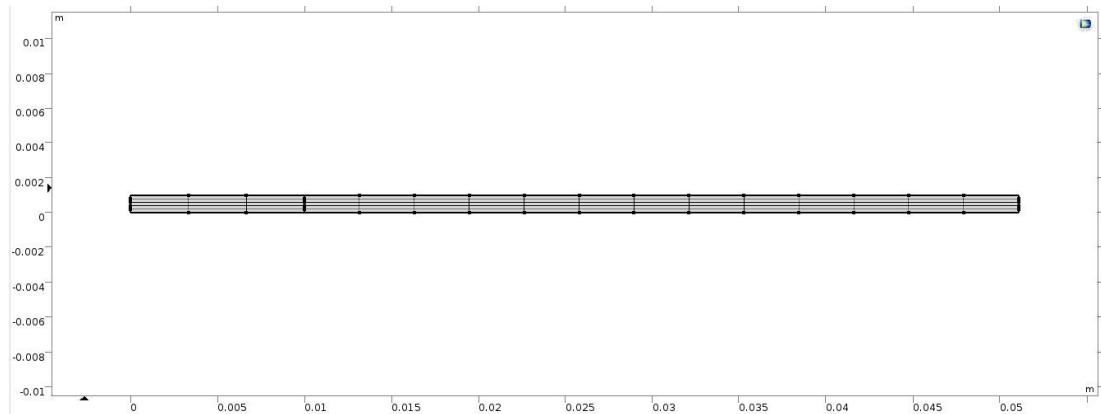


Figure 3.7: 2D IPMC mesh.

3.4.7 Define Study Steps and Compute

The Eigenfrequency study is to determine the natural frequency by load struck on the IPMC boundary. The study was set with 6 step desired of eigenfrequency and computed the load applied on IPMC as shown in Figure 3.8.

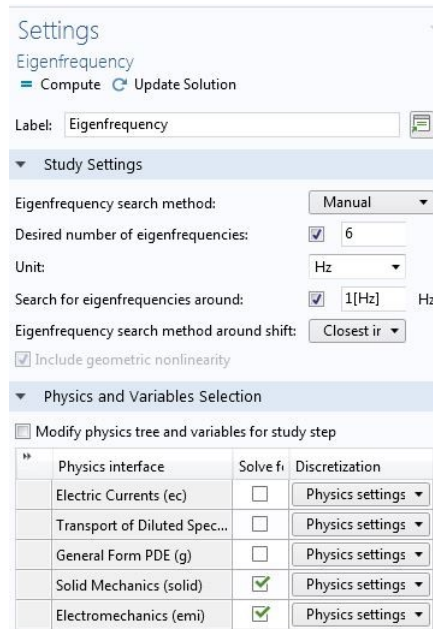


Figure 3.8: Eigenfrequency study setting.

3.5 Summary

The study of cantilever IPMC sensor simulation using COMSOL Multiphysics was done by applying Solid Mechanics for the movement of out of plane by applied force on the IPMC sensor and Electromechanical physics to measure the voltage signal that been produced. Eigenfrequency study used in this simulation by applying six steps of frequency to retrieve all simulation results.

CHAPTER 4

RESULTS AND DISCUSSIONS

4.1 Introduction

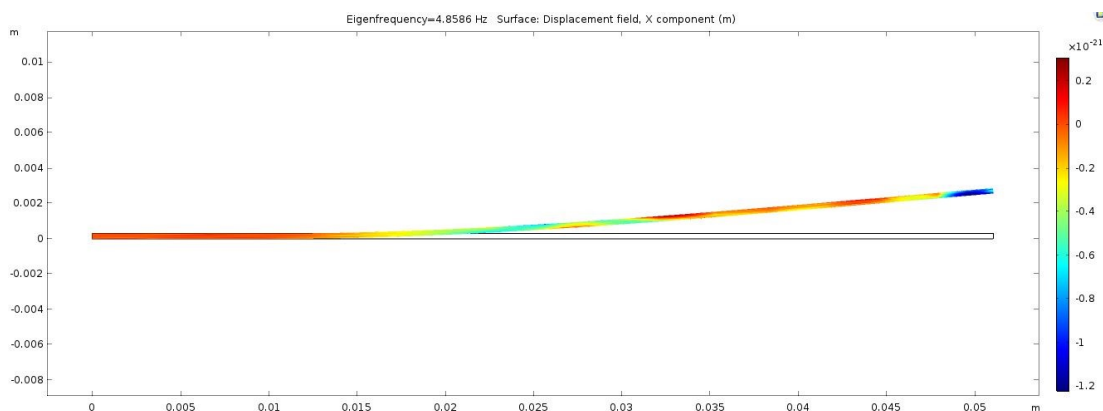
The Comsol Multiphysic simulation result of 2D cantilever IPMC sensor geometry was analyzed with Eigenfrequency study in this chapter. The load applied at IPMC boundary together with the six steps of frequency will create movement and produced voltage signal. The result was plotted into Voltage versus displacement.

4.2 Simulation Result

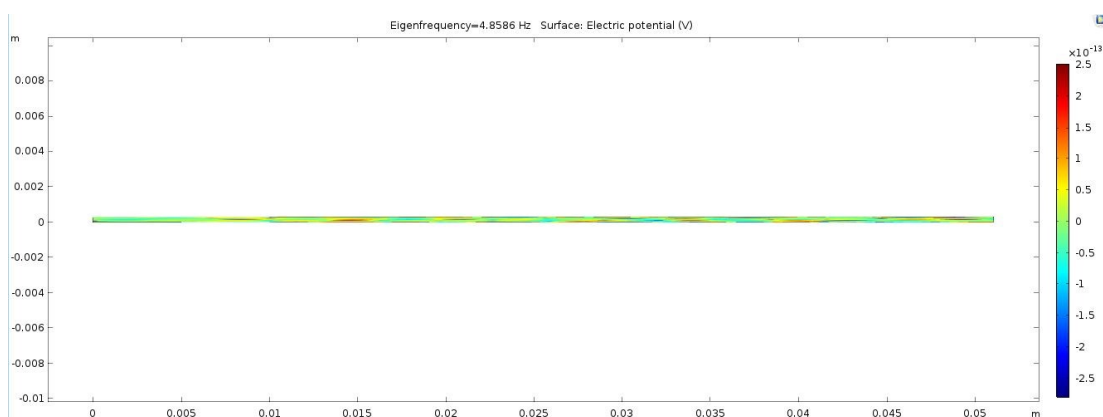
The displacement and deformation of IPMC sensor, resulting from the load applied to the boundary surface and the result divided with thickness variable and eigenfrequency on each number of step mode display as below.

4.2.1 0.29 mm IPMC height result

The 1st step mode of eigenfrequency at 0.29 mm height shown Figure 4.1 below with resulting at 4.96 Hz with the IPMC tilted upward. The red region at Figure 4.1 (A) showed the fixed boundary hold the free moving tips of IPMC.



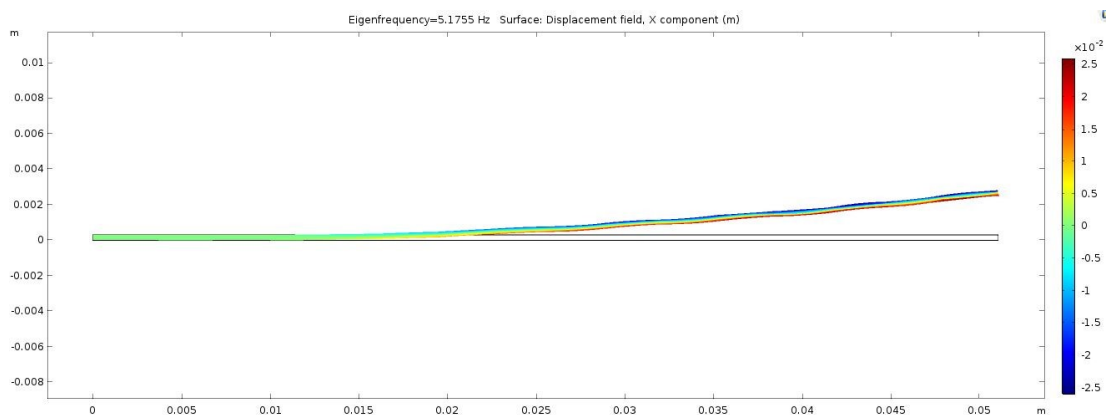
(A)



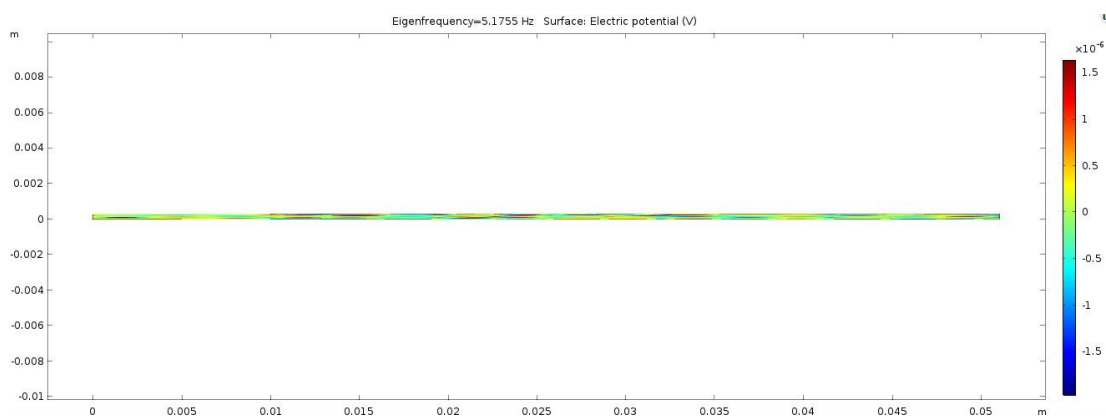
(B)

Figure 4.1: IPMC sensor Eigenfrequency at step mode 1 with result 4.86 Hz, (A) displacement field, m, (B) Electric potential, V.

The 2nd step mode of eigenfrequency at 0.29 mm height shown Figure 4.2 below with resulting at 5.18 Hz with the corrugate shape IPMC tilted upward.



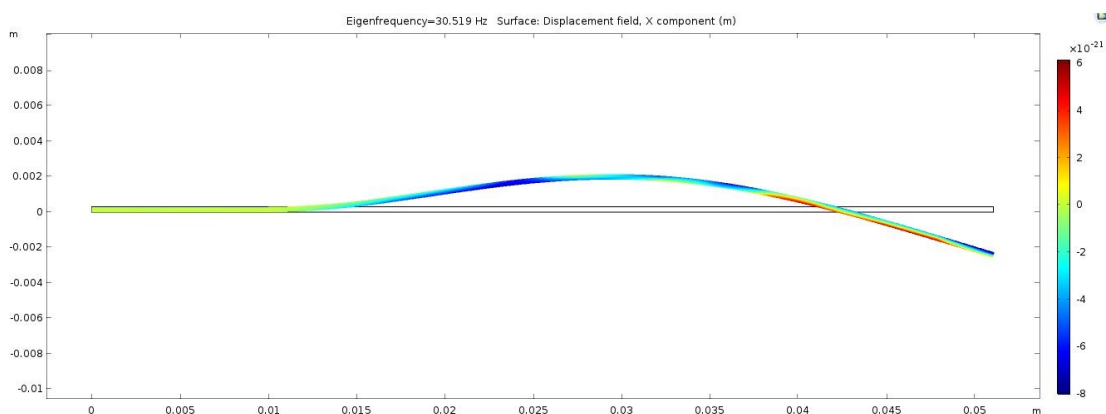
(A)



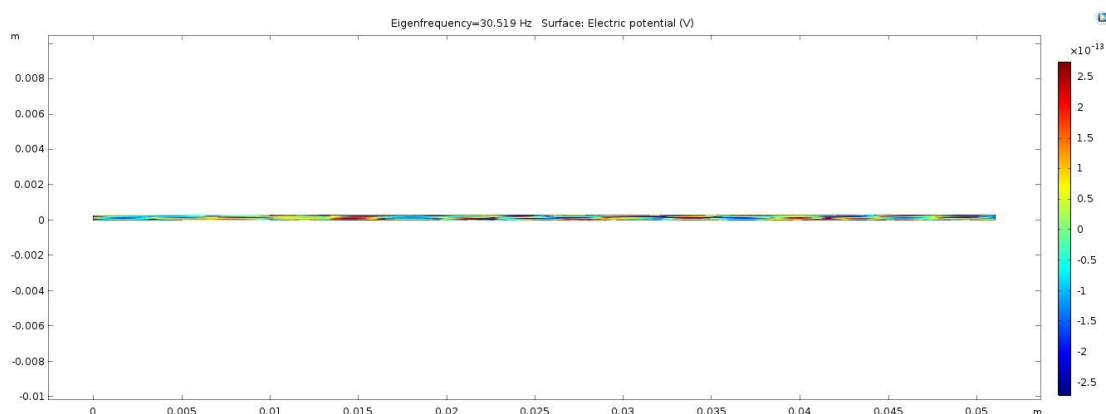
(B)

Figure 4.2: IPMC sensor Eigenfrequency at step mode 2 with result 5.18 Hz, (A) displacement field, m, (B) Electric potential, V.

The 3rd step mode of eigenfrequency at 0.29 mm height shown Figure 4.3 below with resulting at 5.18 Hz with the downward curve shape IPMC.



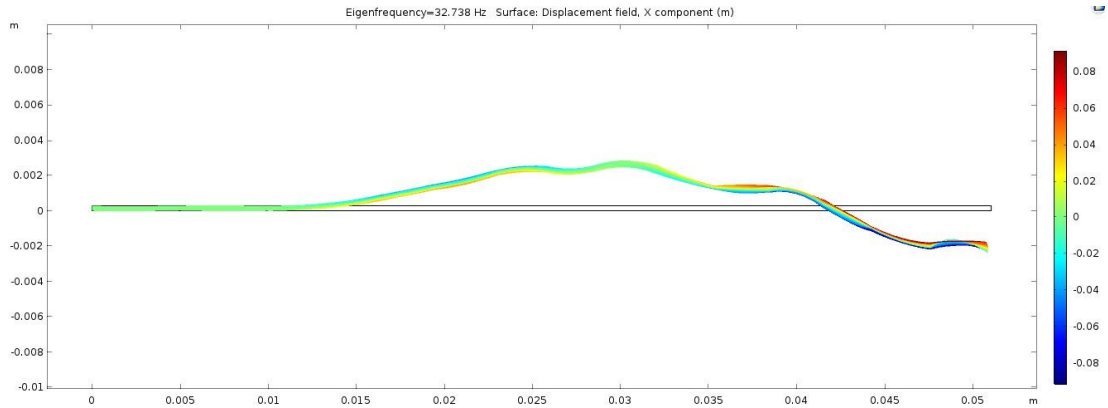
(A)



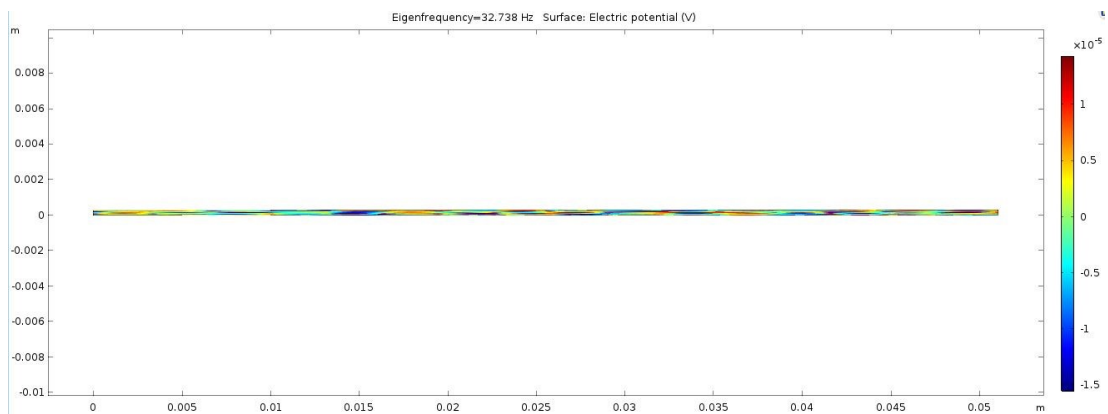
(B)

Figure 4.3: IPMC sensor Eigenfrequency at step mode 3 with result 30.52 Hz, (A) displacement field, m, (B) Electric potential, V.

The 4th step mode of eigenfrequency at 0.29 mm height shown Figure 4.4 below with resulting at 32.74 Hz with the downward curve IPMC. The shape also showed it vibrated due to free movement.



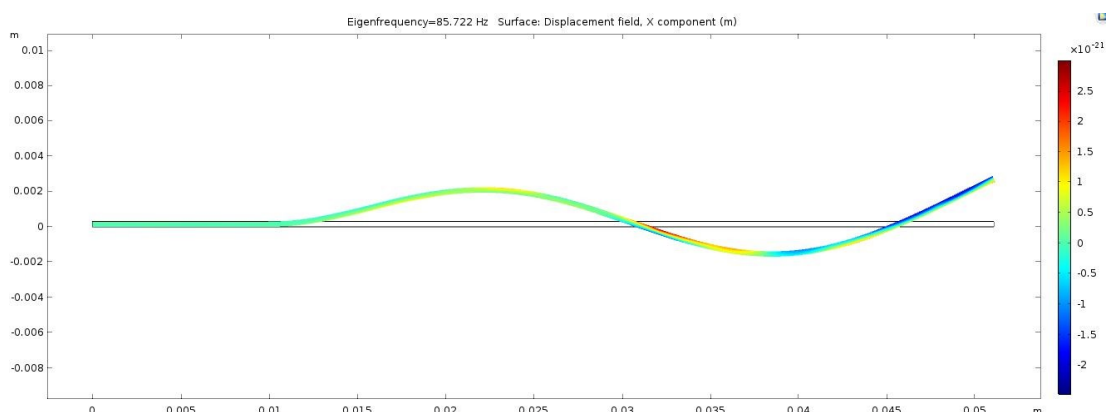
(A)



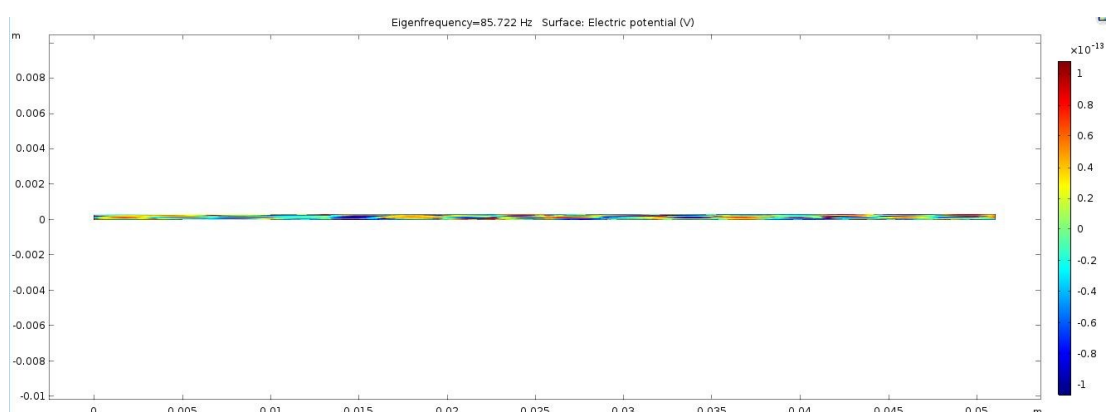
(B)

Figure 4.4: IPMC sensor Eigenfrequency at step mode 4 with result at 32.74 Hz, (A) displacement field, m, (B) Electric potential, V.

The 5th step mode of eigenfrequency at 0.29 mm height shown Figure 4.5 below with resulting at 85.72 Hz with the ‘S’ shape curve IPMC.



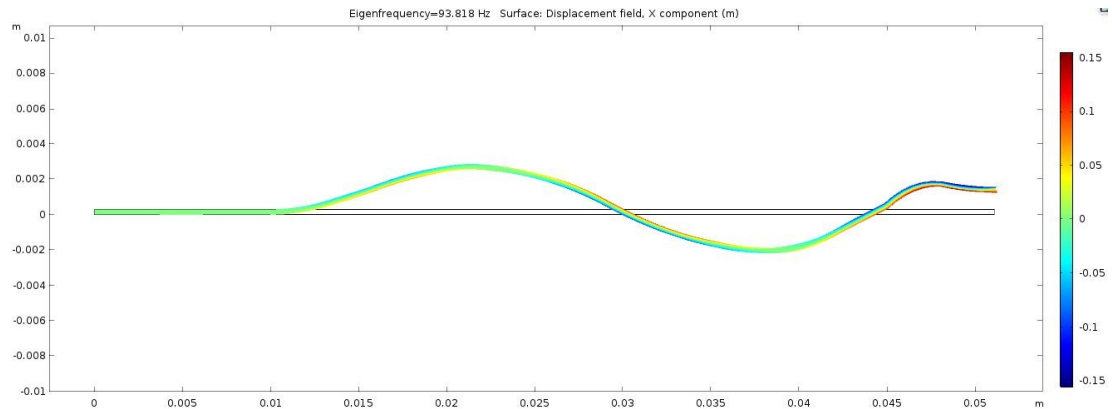
(A)



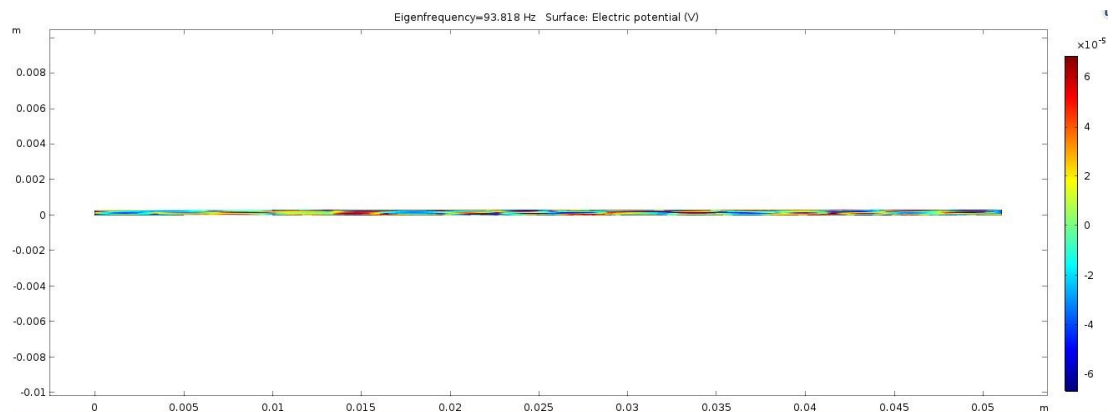
(B)

Figure 4.5: IPMC sensor Eigenfrequency at step mode 5 with result at 85.72 Hz, (A) displacement field, m, (B) Electric potential, V.

The 6th step mode of eigenfrequency at 0.29 mm height shown Figure 4.6 below with resulting at 93.82 Hz with the 'M' shape curve IPMC.



(A)



(B)

Figure 4.6: IPMC sensor Eigenfrequency at step mode 6 with result at 93.82 Hz, (A) displacement field, m, (B) Electric potential, V.

Graph voltage (V) versus displacement (m) was plotted to observe the characteristic of IPMC sensor. Point load at location 10 was assign in Figure 4.7 and the graph shown on Figure 4.8. The voltage is at range 0 V to 1.5 μV .

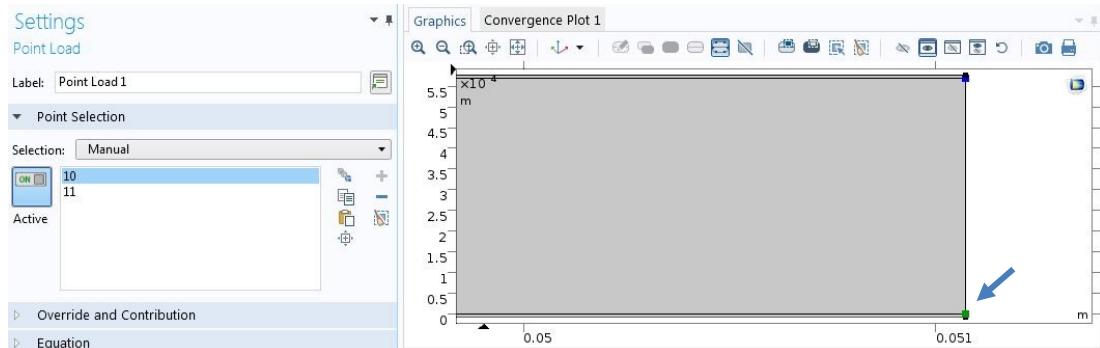


Figure 4.7: Point load at point 10 mark location.

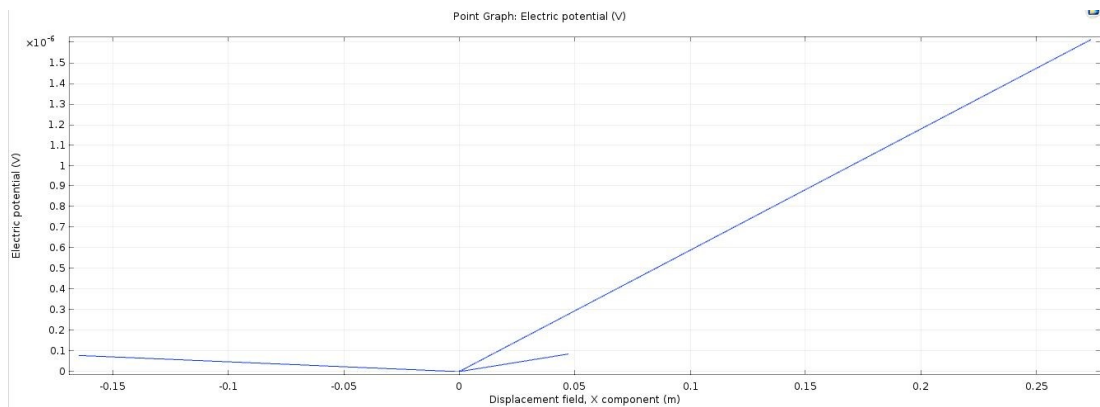


Figure 4.8: Point load at point 10 mark location graph.

Point load at 11 in Figure 4.8. Graph on each point load 10 and 11 as shown in Figure 4.9 and Figure 4.10. The voltage is at range 0 to $9\mu\text{V}$.

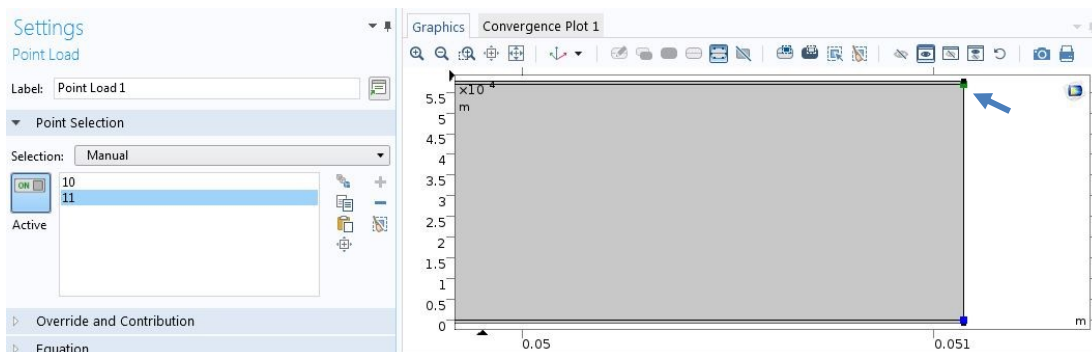


Figure 4.9: Point load at point 11 mark location.

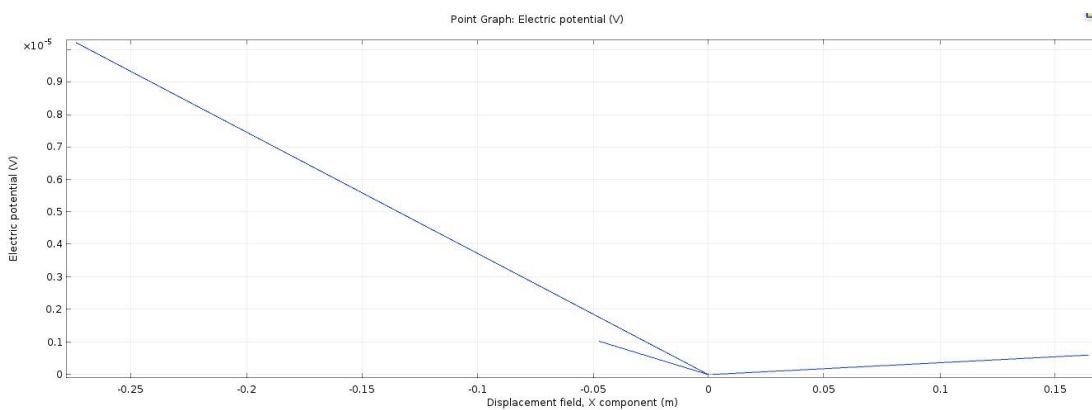
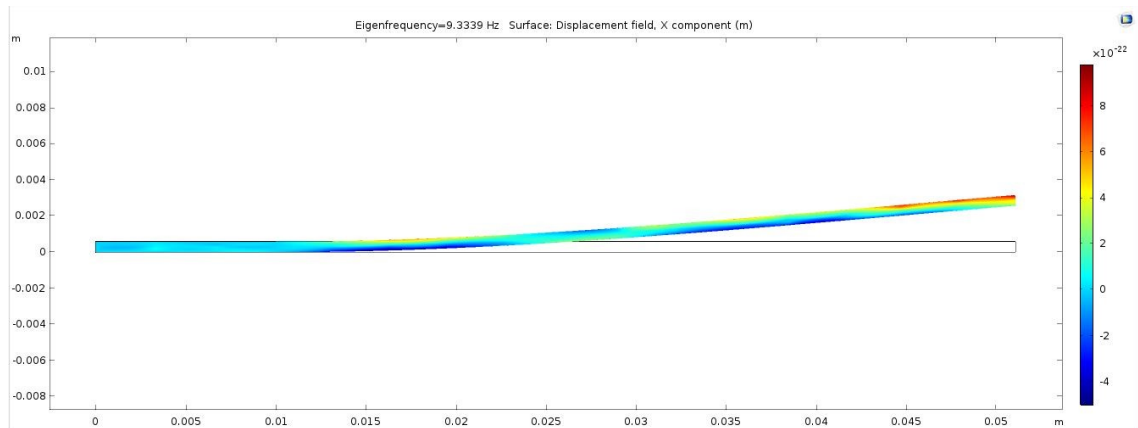


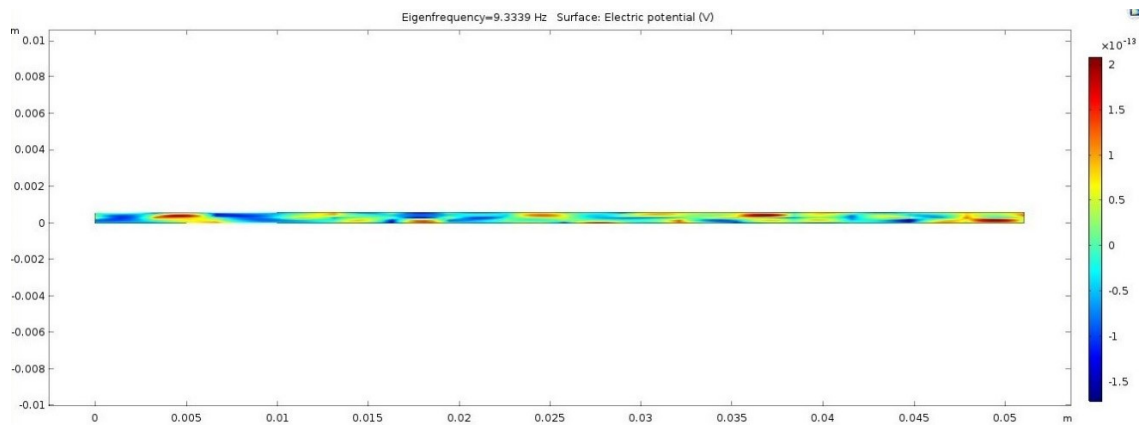
Figure 4.10: Point load at point 11 mark location graph.

4.2.2 0.57 mm IPMC height result

The 1st step mode of eigenfrequency at 0.57 mm height shown Figure 4.11 below with resulting at 9.30 Hz with the IPMC tilted upward.



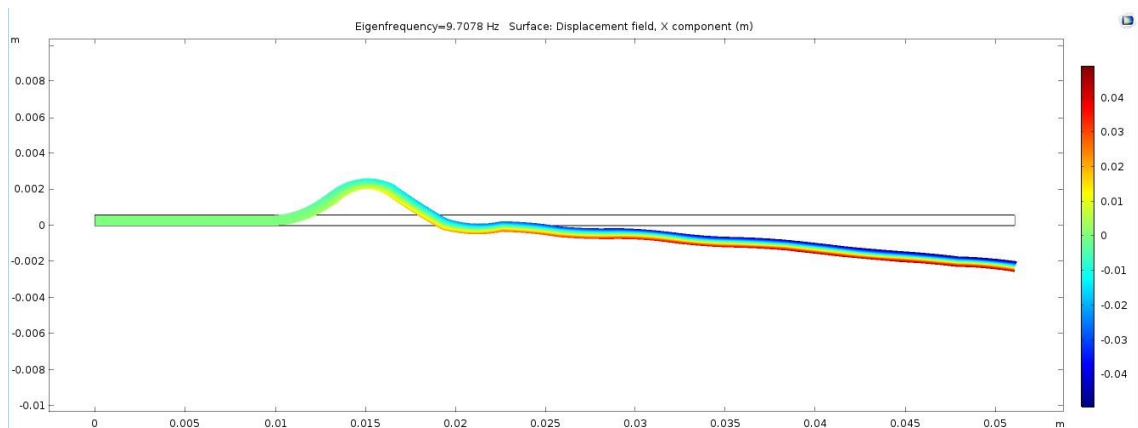
(A)



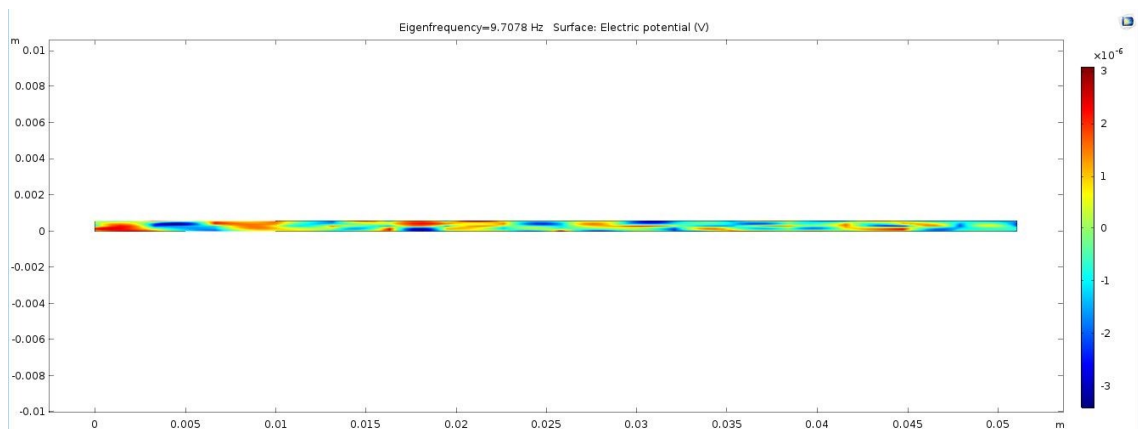
(B)

Figure 4.11: IPMC sensor Eigenfrequency at step mode 1 with result at 9.34Hz, (A) displacement field, m, (B) Electric potential, V.

The 2nd step mode of eigenfrequency at 0.57 mm height shown Figure 4.12 below with resulting at 9.71 Hz with the 'P' shape IPMC downward on tip.



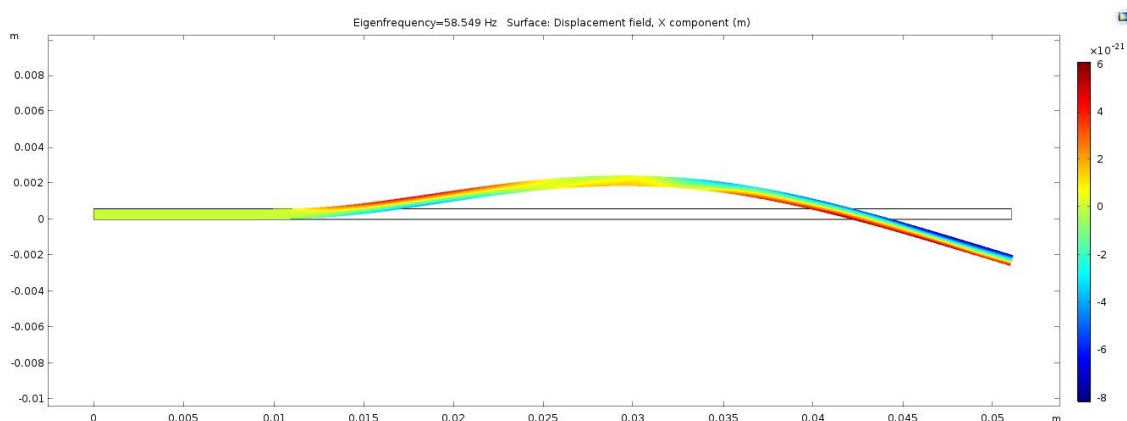
(A)



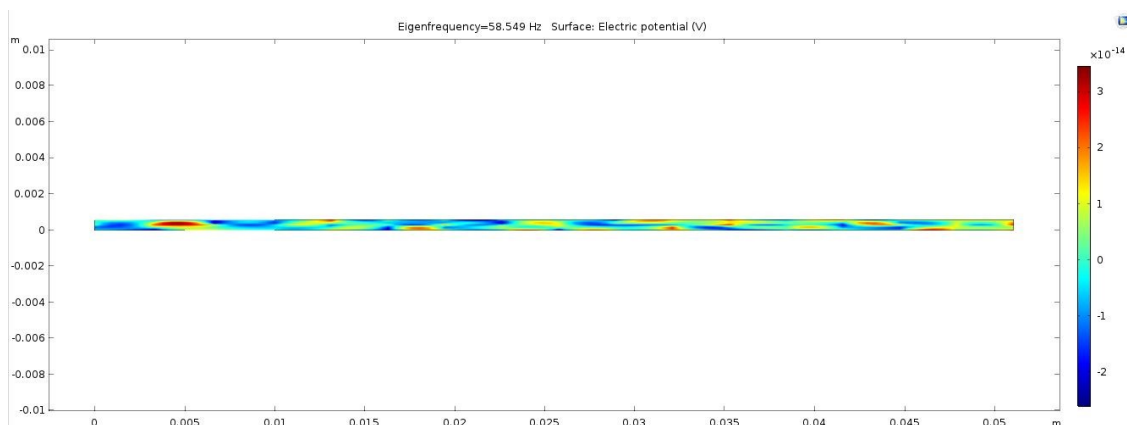
(B)

Figure 4.12: IPMC sensor Eigenfrequency at step mode 2 with result at 9.71Hz, (A) displacement field, m, (B) Electric potential, V.

The 3rd step mode of eigenfrequency at 0.57 mm height shown Figure 4.13 below with resulting at 58.55 Hz with the downward curve shape IPMC.



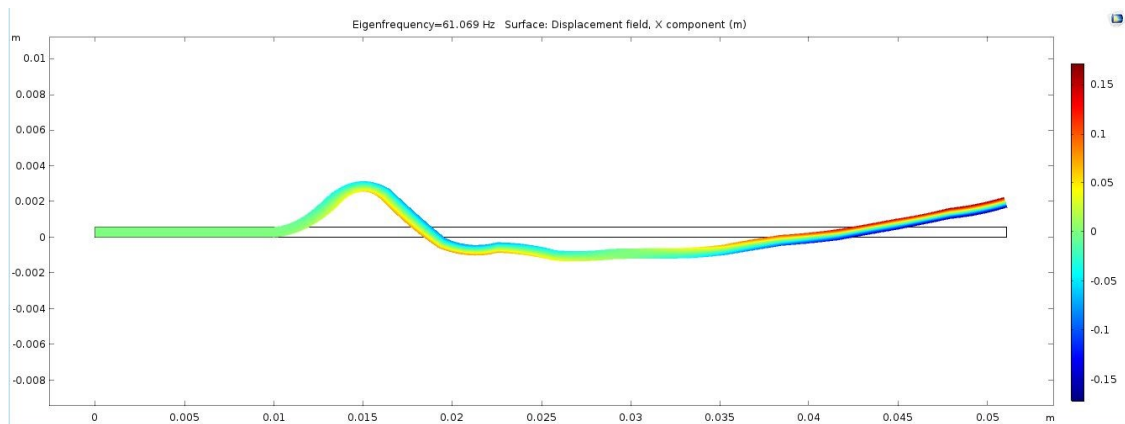
(A)



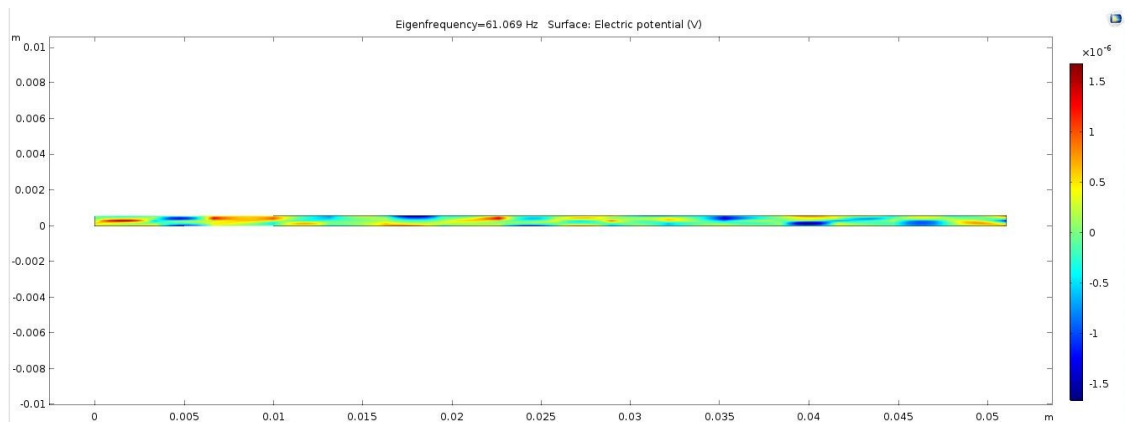
(B)

Figure 4.13: IPMC sensor Eigenfrequency at step mode 3 with result at 58.55 Hz, (A) displacement field, m, (B) Electric potential, V.

The 4th step mode of eigenfrequency at 0.57 mm height shown Figure 4.14 below with resulting at 61.07 Hz with the 'P' shape IPMC upward on tip.



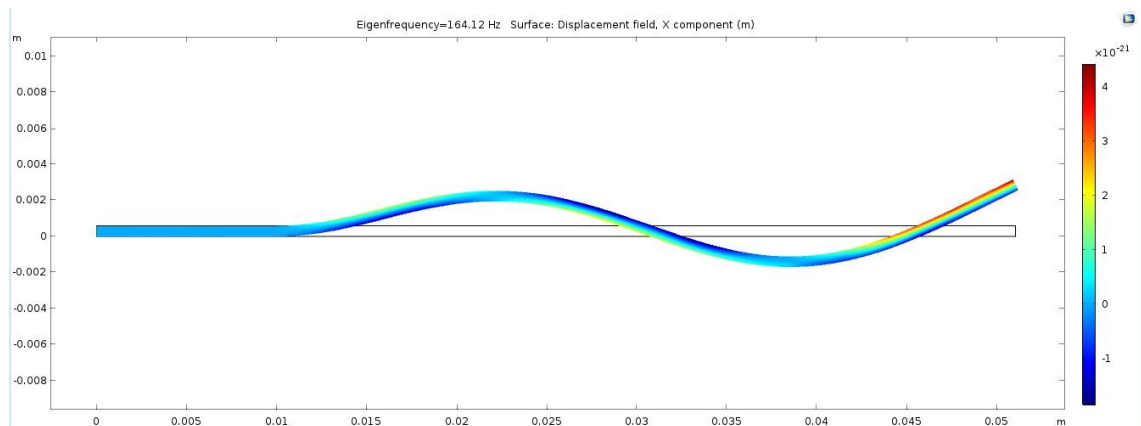
(A)



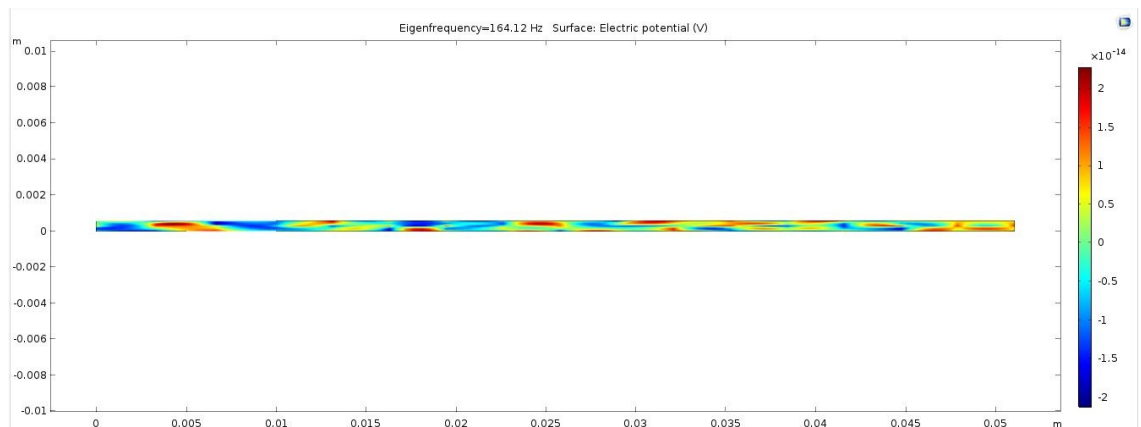
(B)

Figure 4.14: IPMC sensor Eigenfrequency at step mode 4 with result at 61.07Hz, (A) displacement field, m, (B) Electric potential, V.

The 5th step mode of eigenfrequency at 0.57 mm height shown Figure 4.15 below with resulting at 164.12 Hz with the ‘S’ shape IPMC.



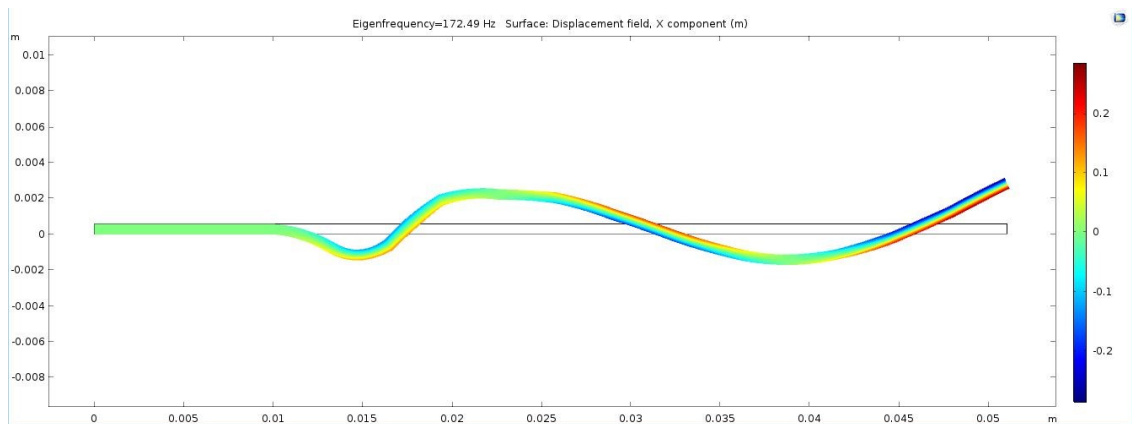
(A)



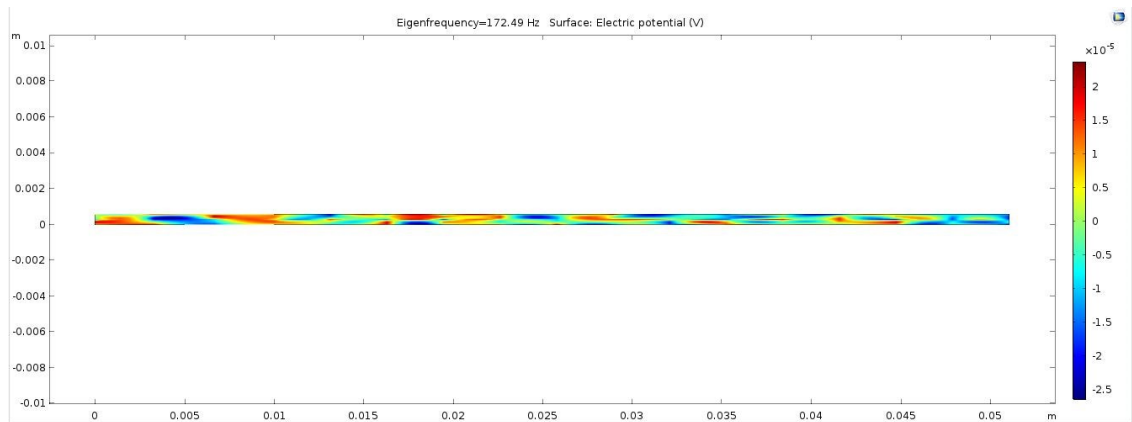
(B)

Figure 4.15: IPMC sensor Eigenfrequency at step mode 5 with result at 164.12 Hz, (A) displacement field, m, (B) Electric potential, V.

The 6th step mode of eigenfrequency at 0.57 mm height shown Figure 4.16 below with resulting at 172.49 Hz with the ‘S’ shape IPMC.



(A)



(B)

Figure 4.16: IPMC sensor Eigenfrequency at step mode 6 with result at 172.49Hz, (A) displacement field, m, (B) Electric potential, V.

Graph voltage (V) versus displacement (m) was plotted to observe the characteristic of IPMC sensor. Point load at 10 was assign and graph was plot at Figure 4.17 with voltage is at range at $-0.05 \mu\text{V}$ to $0.4 \mu\text{V}$. Graph at point 11 in Figure 4.18 with voltage is at range at $-17 \mu\text{V}$ to $2 \mu\text{V}$.

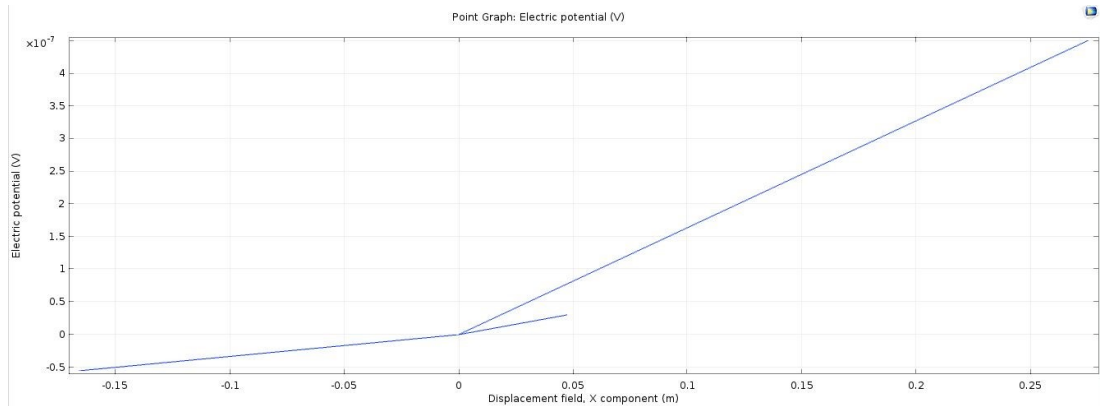


Figure 4.17: Point load at point 10 mark location graph.

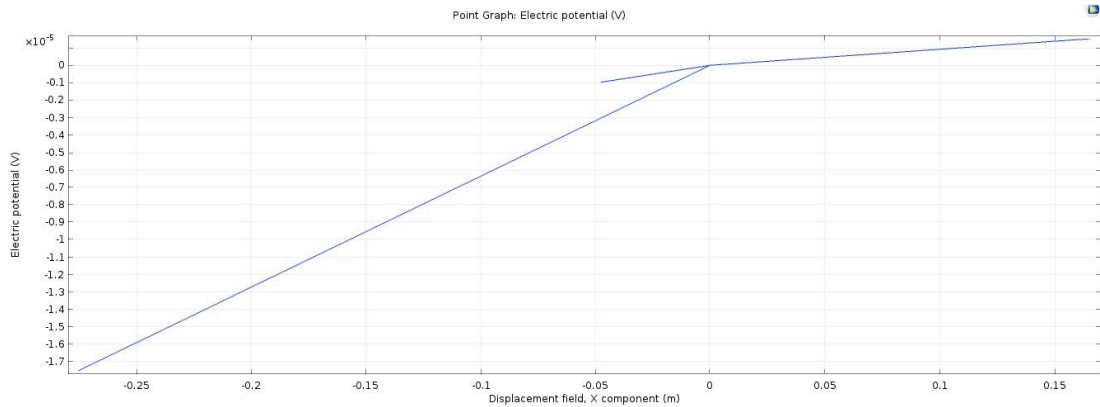
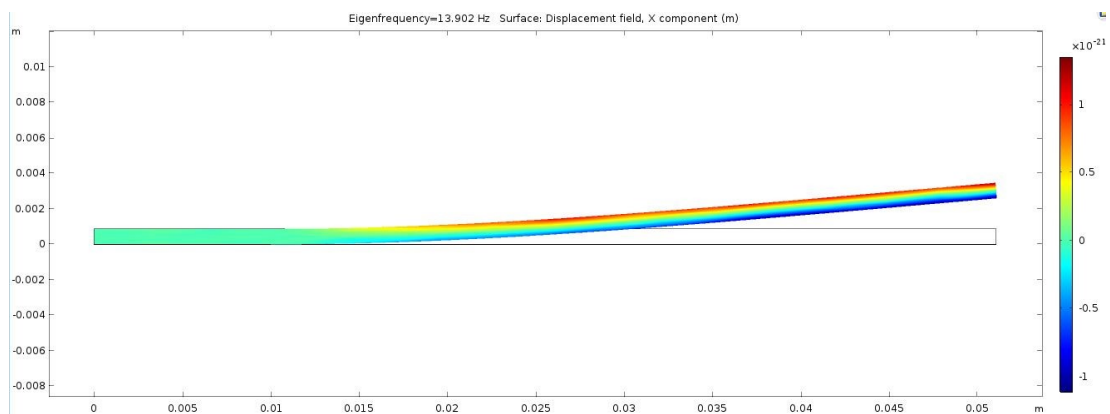


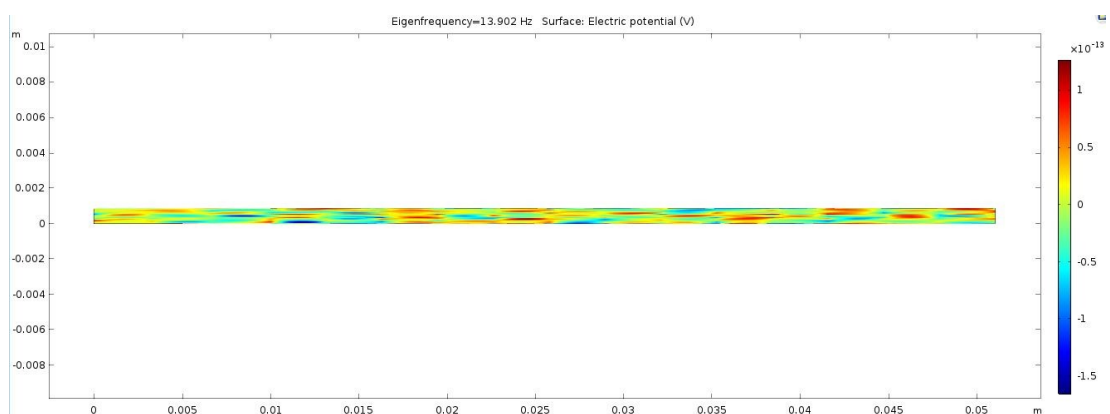
Figure 4.18: Point load at point 11 mark location graph.

4.2.3 0.86 mm IPMC height result

The 1st step mode of eigenfrequency at 0.86 mm height shown Figure 4.19 below with resulting at 13.90 Hz with the IPMC tip tilted upward.



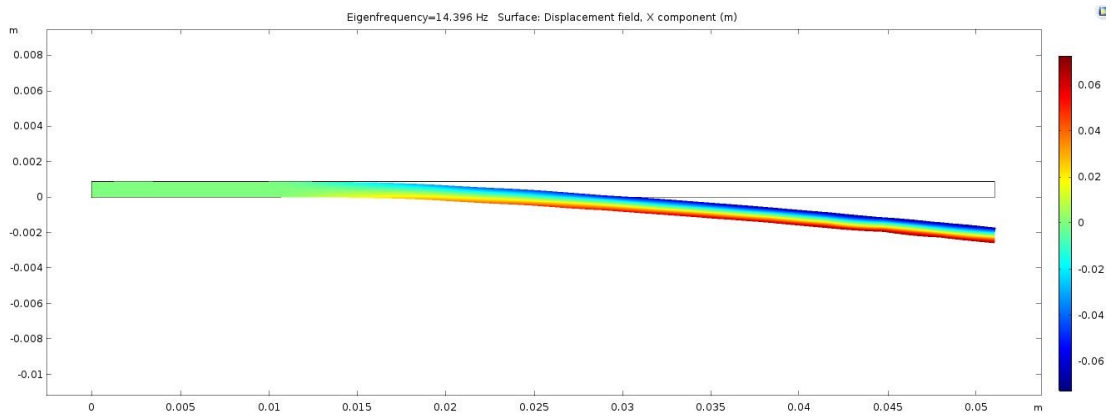
(A)



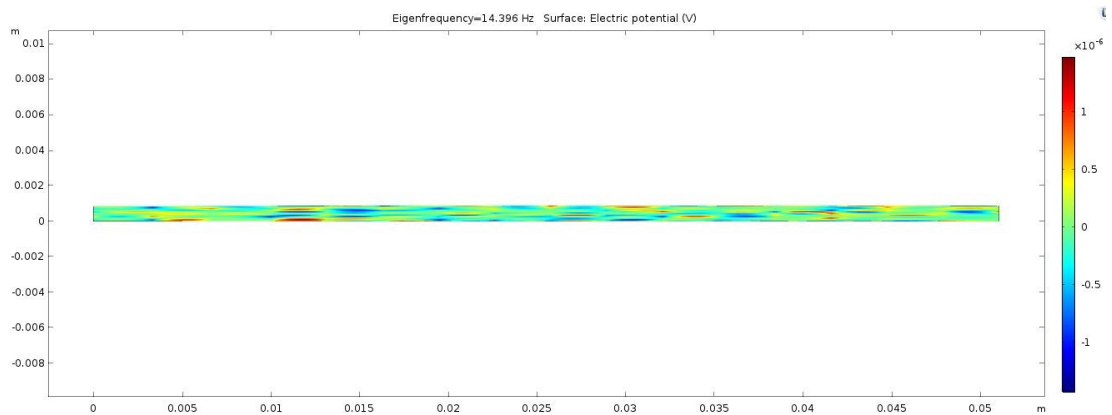
(B)

Figure 4.19: IPMC sensor Eigenfrequency at step mode 1 with result at 13.90 Hz, (A) displacement field, m, (B) Electric potential, V.

The 2nd step mode of eigenfrequency at 0.86 mm height shown Figure 4.20 below with resulting at 14.39 Hz with IPMC tip tilted downward.



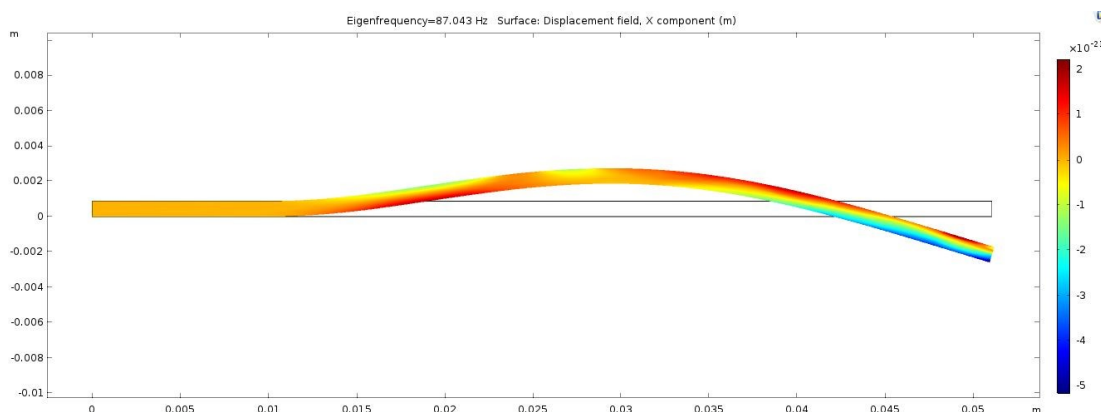
(A)



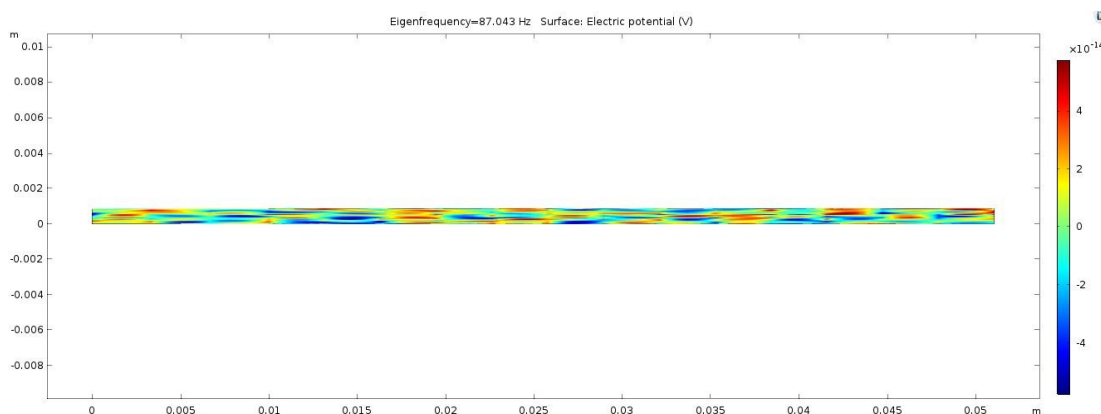
(B)

Figure 4.20: IPMC sensor Eigenfrequency at step mode 2 with result at 14.39 Hz, (A) displacement field, m, (B) Electric potential, V.

The 3rd step mode of eigenfrequency at 0.86 mm height shown Figure 4.21 below with resulting at 87.04 Hz with the downward curve shape IPMC.



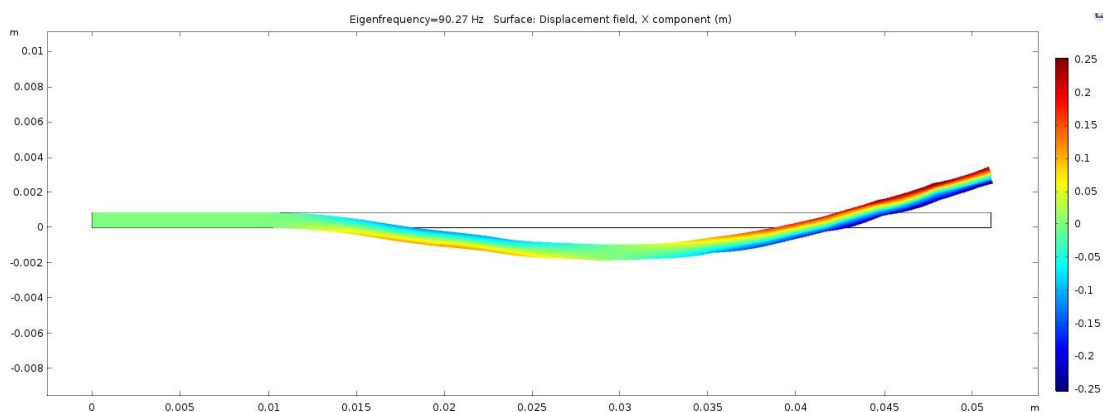
(A)



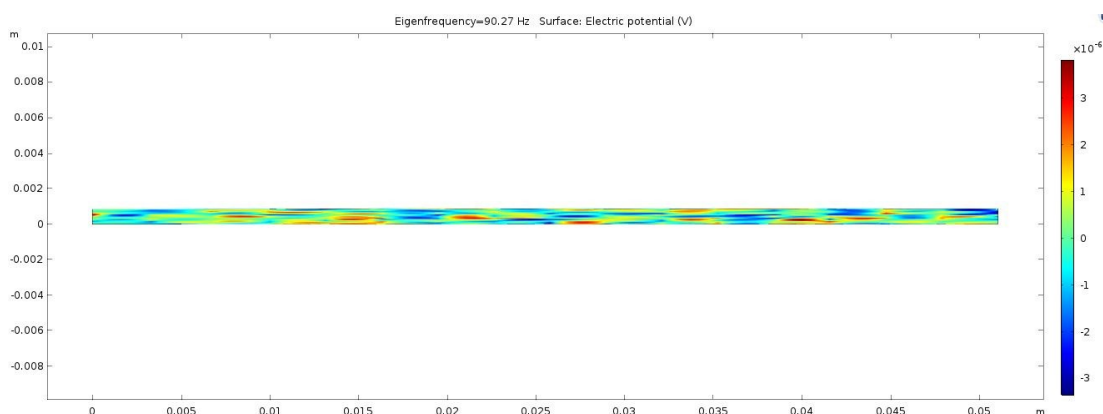
(B)

Figure 4.21: IPMC sensor Eigenfrequency at step mode 3 with result at 87.04 Hz, (A) displacement field, m, (B) Electric potential, V.

The 4th step mode of eigenfrequency at 0.86 mm height shown Figure 4.22 below with resulting at 90.27 Hz with the upward curve shape IPMC.



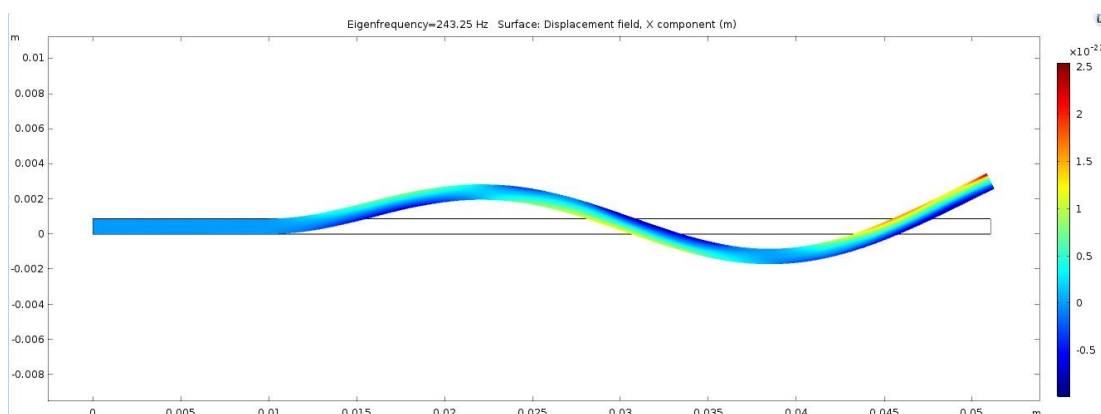
(A)



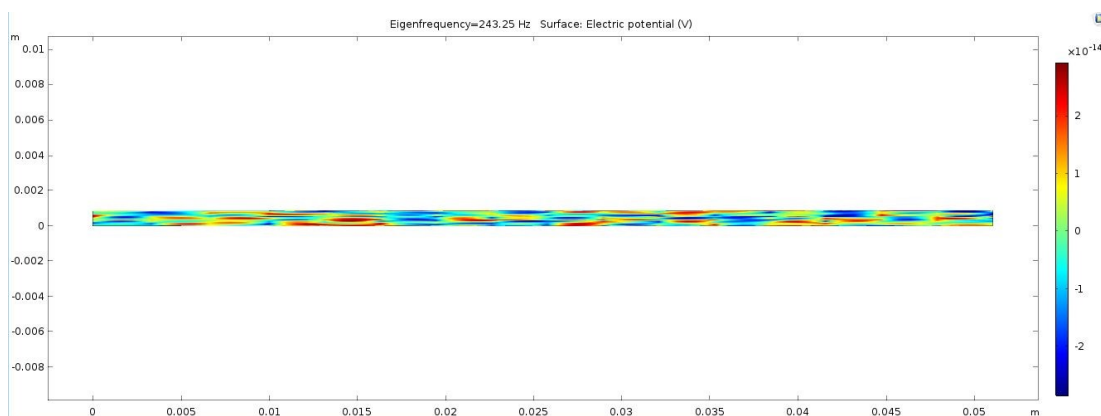
(B)

Figure 4.22: IPMC sensor Eigenfrequency at step mode 4 with result at 90.27 Hz, (A) displacement field, m, (B) Electric potential, V.

The 5th step mode of eigenfrequency at 0.86 mm height shown Figure 4.23 below with resulting at 243.25 Hz with the ‘S’ shape IPMC.



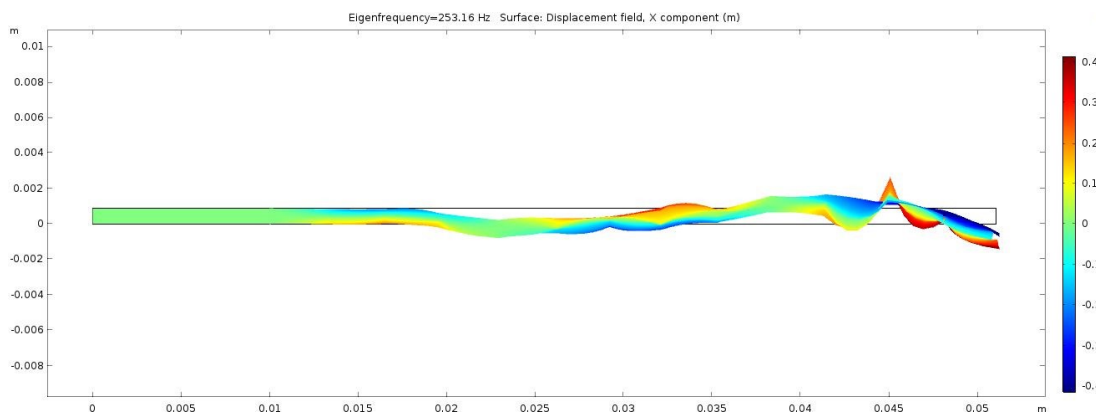
(A)



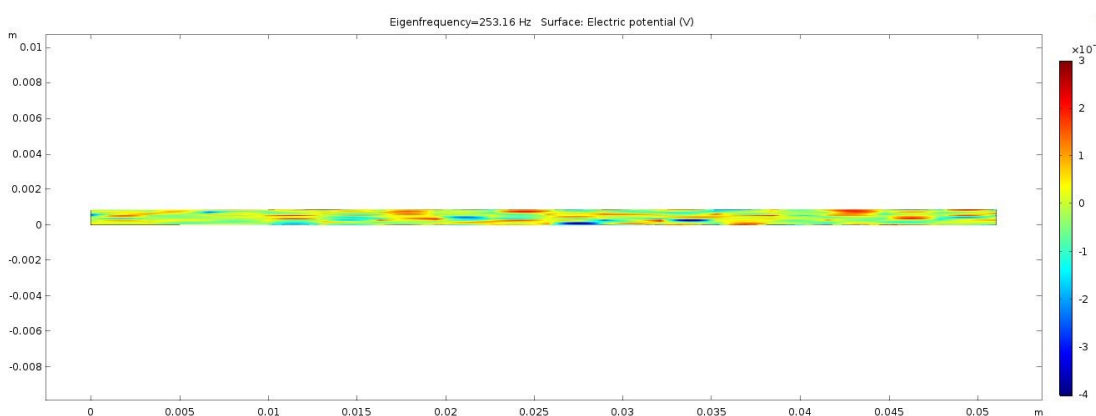
(B)

Figure 4.23: IPMC sensor Eigenfrequency at step mode 5 with result at 243.25 Hz, (A) displacement field, m, (B) Electric potential, V.

The 6th step mode of eigenfrequency at 0.57 mm height shown Figure 4.24 below with resulting at 253.16 Hz with curvy shape IPMC.



(A)



(B)

Figure 4.24: IPMC sensor Eigenfrequency at step mode 6 with result at 253.16Hz, (A) displacement field, m, (B) Electric potential, V.

Graph voltage (V) versus displacement (m) was plotted to observe the characteristic of IPMC sensor. Point load at 10 was assign and graph was plot at Figure 4.25 with voltage is at range at $-0.05 \mu\text{V}$ to $0.45 \mu\text{V}$. Graph at point 11 in Figure 4.18 with voltage is at range at $-17 \mu\text{V}$ to $2 \mu\text{V}$.

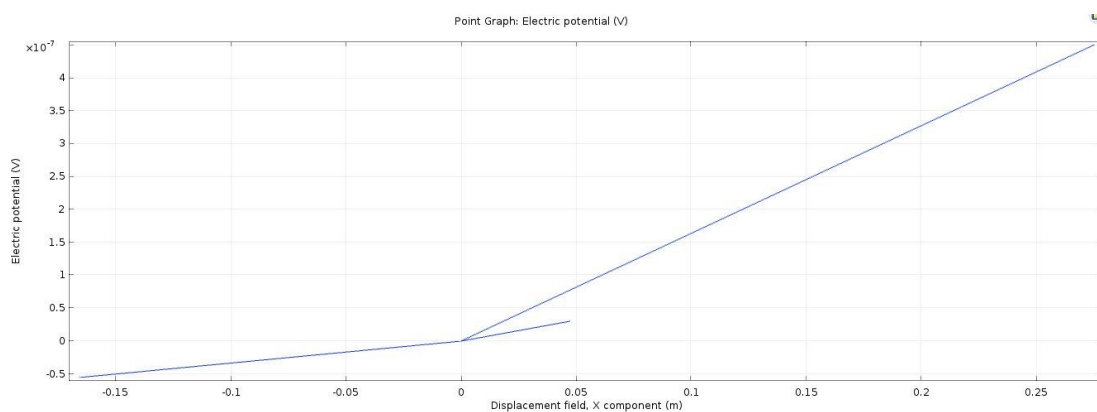


Figure 4.25: Point load at point 10 mark location graph.

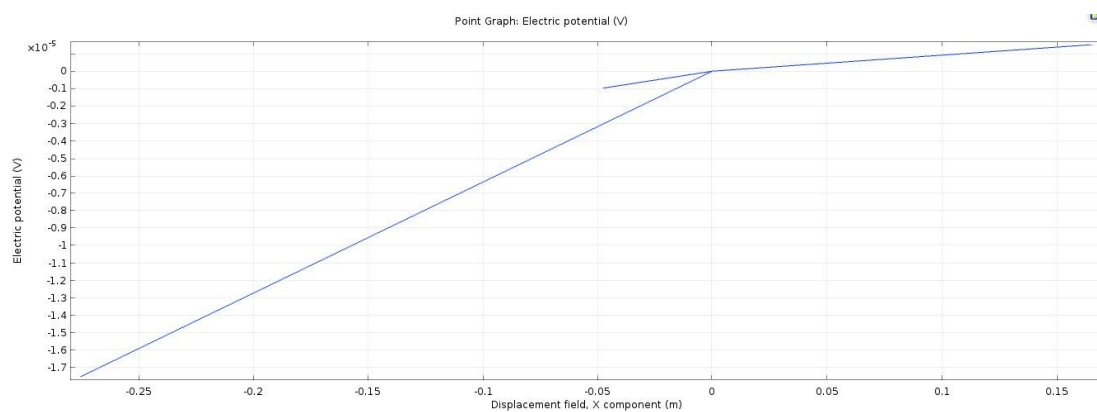


Figure 4.26: Point load at point 11 mark location graph.

Eigenfrequency Mode Number	1	2	3	4	5	6
IPMC Height						
0.29 mm	4.86 Hz	5.18 Hz	30.52 Hz	32.74 Hz	85.72 Hz	93.82 Hz
0.57 mm	9.30 Hz	9.71 Hz	58.36 Hz	61.06 Hz	163.59 Hz	172.43 Hz
0.86 mm	13.90 Hz	14.40 Hz	87.04 Hz	90.27 Hz	243.25 Hz	253.16 Hz

Table 4.1: Eigenfrequency result

4.3 Summary

Result of IPMC sensor showed how it interact between free movement frequency of IPMC tips due to applied loads or out of plane force and voltage signal. The result give an idea how the IPMC sensor can generate voltage signal due to unwanted load or free movement of IPMC beam end tip.

CHAPTER 5

CONCLUSIONS AND RECOMMENDATIONS

5.1 Conclusions

The characteristic of IPMC sensor was studied and result been analysed from the COMSOL Multiphysics version 5.3. Out of plane deformation movement of IPMC generate voltage signal along the IPMC sensor cantilever from the load applied. The IPMC also creates natural frequency due to the free movement of end of tip after applying the single load. The frequency increase if the IPMC height design increase. This showed that the free hanging IPMC can move by load struck on the beam to create an ion migration in IPMC and generate electrical signal and act as energy harvester. This study showed the IPMC sensor can be a better findings for future application.

5.2 Recommendations for future work

IPMC have high potential as sensor. Therefore the study on the corrugate IPMC surface is desirable. The corrugate surface can give different characteristic on IPMC sensor based on electrical signals that generate form the movement of deformation on IPMC sensor.

REFERENCES

1. Abdelnour, K. *et al.* (2012) 'Wireless powering of ionic polymer metal composites toward hovering microswimmers', *IEEE/ASME Transactions on Mechatronics*. IEEE, 17(5), pp. 924–935. doi: 10.1109/TMECH.2011.2148201.
2. Abdulsadda, A. T. and Tan, X. (2012) 'An artificial lateral line system using IPMC sensor arrays', *International Journal of Smart and Nano Materials*, 3(3), pp. 226–242. doi: 10.1080/19475411.2011.650233.
3. AMRITA (2011) 'Free Vibration of a Cantilever Beam (Continuous System)'. Available at: <http://vlab.amrita.edu/?sub=3&brch=175&sim=1080&cnt=1> (Accessed: 13 May 2019).
4. Andò, B. *et al.* (2013) 'A Seismic Sensor Based on IPMC Combined With Ferrofluids', *IEEE Transactions on Instrumentation and Measurement*, VOL. 62, NO. 5, MAY 2013, 62(5), pp. 1292–1298.
5. Annabestani, M., Maymandi-Nejad, M. and Naghavi, N. (2016) 'Restraining IPMC Back Relaxation in Large Bending Displacements: Applying Non-Feedback Local Gaussian Disturbance by Patterned Electrodes', *IEEE Transactions on Electron Devices*, 63(4), pp. 1689–1695. doi: 10.1109/TED.2016.2530144.
6. Arena, P. *et al.* (2006) 'Design and control of an IPMC wormlike robot', *IEEE Transactions on Systems, Man, and Cybernetics, Part B: Cybernetics*, 36(5), pp. 1044–1052. doi: 10.1109/TSMCB.2006.873188.
7. Bar-cohen, Y. (2002) 'Electro-active polymers: current capabilities and challenges', in *Proceedings of the SPIE Smart Structures and Materials Symposium, EAPAD Conference, San Diego, CA*, p. Paper 4695-02.
8. Bar-cohen, Y. (2004) *Electroactive Polymer (EAP) Actuators as Artificial Muscles: Reality, Potential, and Challenges. Second Edi.* Edited by Y. Bar-cohen. SPIE PRESS.
9. Bhandari, B., Lee, G. Y. and Ahn, S. H. (2012) 'A review on IPMC material as actuators and sensors: Fabrications, characteristics and applications', *International Journal of Precision Engineering and Manufacturing*, 13(1), pp. 141–163. doi: 10.1007/s12541-012-0020-8.
10. Bonomo, C. *et al.* (2008) 'A Tactile Sensor for Biomedical Applications Based on IPMCs', *IEEE Sensor Journal*, VOL. 8, NO. 8, AUGUST 2008, 8(8), pp. 1486–

1493.

11. Brunetto, P. *et al.* (2010) ‘A resonant vibrating tactile probe for biomedical applications based on IPMC’, *IEEE Transactions on Instrumentation and Measurement*, 59(5), pp. 1453–1462. doi: 10.1109/TIM.2009.2038297.
12. Brunetto, P. *et al.* (2011) ‘Characterization of the temperature and humidity influence on ionic polymer-metal composites as sensors’, *IEEE Transactions on Instrumentation and Measurement*. IEEE, 60(8), pp. 2951–2959. doi: 10.1109/TIM.2011.2118870.
13. Chattaraj, R. *et al.* (2018) ‘Soft wearable ionic polymer sensors for palpatory pulse-rate extraction’, *Sensors and Actuators, A: Physical*. Elsevier B.V., 270, pp. 65–71. doi: 10.1016/j.sna.2017.12.041.
14. COMSOL (2018) 'Eigenfrequency Analysis', *Comsol Multiphysics Cyclopedia*. Available at: <https://www.comsol.com/multiphysics/eigenfrequency-analysis> (Accessed: 12 May 2019).
15. Coombs, S. and Braun, C. B. (2003) ‘Information Processing by the Lateral Line System BT - Sensory Processing in Aquatic Environments’, in *Collin, S. P. and Marshall, N. J. (eds). New York, NY: Springer New York*, pp. 122–138. doi: 10.1007/978-0-387-22628-6_7.
16. Feng, G. H. and Yen, S. C. (2016) ‘Arch-Shaped Ionic Polymer-Metal Composite Actuator Integratable with Micromachined Functional Tools for Micromanipulation’, *IEEE Sensors Journal*, 16(19), pp. 7109–7115. doi: 10.1109/JSEN.2016.2597861.
17. Feng, G. and Huang, W. (2016) ‘Lab on a Soft Robot: Electrically Controlled Tuning Fork Shape IPMC Clamping Actuator With Ultrasonic Imaging and Displacement Self Detecting Capabilities’, *2013 Transducers & Eurosensors XXVII: The 17th International Conference on Solid-State Sensors, Actuators and Microsystems*, (January), pp. 391–398.
18. Gudarzi, M., Smolinski, P. and Wang, Q. M. (2017) ‘Compression and shear mode ionic polymer-metal composite (IPMC) pressure sensors’, *Sensors and Actuators, A: Physical*. Elsevier B.V., 260, pp. 99–111. doi: 10.1016/j.sna.2017.04.010.
19. HDI Solution INC (2016) 'Basic Principle of a Scanning Acoustic Tomograph'. Available at: <http://www.hdi-solutions.com/products/Brochures/SATBasics.pdf>.
20. Hemsell, T. *et al.* (2007) ‘Resonant vibrating sensors for tactile tissue

- differentiation’, *Journal of Sound and Vibration*, 308(3–5), pp. 441–446. doi: 10.1016/j.jsv.2007.03.063.
21. Hubbard, J. J. *et al.* (2014) ‘Monolithic IPMC fins for propulsion and maneuvering in bioinspired underwater robotics’, *IEEE Journal of Oceanic Engineering*, 39(3), pp. 540–551. doi: 10.1109/JOE.2013.2259318.
 22. Lei, H., Sharif, M. A. and Tan, X. (2016) ‘Dynamics of omnidirectional IPMC sensor: Experimental characterization and physical modeling’, *IEEE/ASME Transactions on Mechatronics*, 21(2), pp. 601–612. doi: 10.1109/TMECH.2015.2468080.
 23. Macquarie University (2009) Standing Waves and Resonance. Available at: <https://www.mq.edu.au/about/about-the-university/faculties-and-departments/faculty-of-human-sciences/departments-and-centres/department-of-linguistics/our-research/phonetics-and-phonology/speech/acoustics/acoustic-theory-of-speech-production/standing-waves-and-resonance> (Accessed: 13 May 2019).
 24. Manuel, T. L. and Voth, D. (2014) ‘Nature ’ s Guide to Robot’, *IEEE Intelligent Systems (Volume: 17 , Issue: 6 , Nov.-Dec. 2002)*, pp. 4–6. doi: 10.1109/MIS.2002.1134354.
 25. McDaid, A. J. *et al.* (2012) ‘Control of IPMC actuators for microfluidics with adaptive “online” iterative feedback tuning’, *IEEE/ASME Transactions on Mechatronics*, 17(4), pp. 789–797. doi: 10.1109/TMECH.2011.2135373.
 26. Nam, D. N. C. and Ahn, K. K. (2012) ‘Design of an IPMC diaphragm for micropump application’, *Sensors and Actuators, A: Physical*. Elsevier B.V., 187, pp. 174–182. doi: 10.1016/j.sna.2012.08.027.
 27. Ngoc, D. *et al.* (2012) ‘A novel design technique for IPMC diaphragm in micropump application’, *12th International Conference on Control, Automation and Systems*. IEEE, pp. 360–365.
 28. Nguyen, K. T. *et al.* (2015) ‘Terrestrial Walking Robot with 2DoF Ionic Polymer-Metal Composite (IPMC) Legs’, *IEEE/ASME Transactions on Mechatronics*. IEEE, 20(6), pp. 2962–2972. doi: 10.1109/TMECH.2015.2419820.
 29. Ostrowski, J. P. and Burdick, A. (1998) ‘The Mechanics and Control of Undulatory Locomotion’, *International Journal of Robotics Research*, 17(7), pp. 683–701. Available at: papers://dc655b36-91f1-4c2b-88b1-0972dfc51324/Paper/p1967.

30. Porfiri, M. (2008) 'Charge dynamics in ionic polymer metal composites', *Journal of Applied Physics*. doi: 10.1063/1.3017467.
31. Pugal, D. *et al.* (2016) 'Modeling Ionic Polymer Metal Composites with COMSOL : Step-by-Step Guide', in *Ionic Polymer Metal Composites (IPMCs): Smart Multi-Functional Materials and Artificial Muscles, Volume 1*. Royal Society Of Chemistry, pp. 185–214.
32. Shahinpoor, M. *et al.* (1998) 'Ionic Polymer-Metal Composites (IPMC) As Biomimetic Sensors and Actuators', *Annual International Symposium on Smart Structures and Materials*, (3324), pp. 1–17.
33. Shahinpoor, M. *et al.* (2009) 'Ionic Polymer-Metal Composites as Biomimetic Sensors and Actuators-Artificial Muscles', pp. 25–50. doi: 10.1021/bk-1999-0726.ch003.
34. Shahinpoor, M. (2015) 'Ionic Polymer Metal Composites (IPMCs) Smart Multi-Functional Materials and Artificial Muscles Volume 1'. *Edited by M. Shahinpoor*. Royal Society Of Chemistry.
35. Shahinpoor, M. (2016) 'Ionic Polymer Metal Composites (IPMCs) Smart Multi-Functional Materials and Artificial Muscles Volume 2'. *Edited by M. Shahinpoor*. Royal Society Of Chemistry.
36. Stalbaum, T., Shen, Q. and Kim, K. J. (2016) 'Ion Concentration and Electromechanical Actuation Simulations of Ionic Polymer-Metal Composites', in *COMSOL Conference 2016 Boston, Massachusetts, USA*. Available at: https://www.comsol.com/paper/download/363421/stalbaum_presentation.pdf.
37. Strazzeri, S. *et al.* (2009) 'Static and Dynamic Characterization of the Temperature and Humidity Influence on IPMC Actuators', *IEEE Transactions on Instrumentation and Measurement*, 59(4), pp. 893–908. doi: 10.1109/tim.2009.2026613.
38. Thomas, K. and Faouzi, M. W. (2016) 'Elastic Moduli of Breast and Prostate Tissues Under Compression', *Ultrasonic Imaging* 20,260-274 (1998), 274(1998), pp. 260–274.
39. Trivedi, D. *et al.* (2008) 'Soft robotics: Biological inspiration, state of the art, and future research', *Applied Bionics and Biomechanics*, 5(3), pp. 99–117. doi: 10.1080/11762320802557865.
40. Tsiakmakis, K. *et al.* (2009) 'A camera based method for the measurement of

- motion parameters of IPMC actuators', *IEEE Transactions on Instrumentation and Measurement*. IEEE, 58(8), pp. 2626–2633. doi: 10.1109/TIM.2009.2015641.
41. Wang, H. *et al.* (2015) 'Motion Planning Based on Learning From Demonstration for Multiple-Segment Flexible Soft Robots Actuated by Electroactive Polymers', *IEEE Robotics And Automation Letter*, VOL. 1, NO. 1, JANUARY 2016, 1(1), pp. 391–398.
42. Wang, J. *et al.* (2017) 'A compact Ionic Polymer-Metal Composite (IPMC) actuated valveless pump for drug delivery', *IEEE/ASME Transactions on Mechatronics*, 22(1), pp. 196–205. doi: 10.1109/TMECH.2016.2624762.